A Defective Vacuolar Proton Pump Enhances Aluminum Tolerance by Reducing Vacuole Sequestration of Organic Acids[1]

Feng Zhang,[a] Xiaoyi Yan,[a] Xingbao Han,[a] Renjie Tang,[b] Moli Chu,[a] Yang Yang,[a] Yong-Hua Yang,[a] Fugeng Zhao,[a] Aigen Fu,[c] Sheng Luan,[b,2] and Wenzhi Lan[a,3]

[a]State Key Laboratory for Pharmaceutical Biotechnology, School of Life Sciences, Nanjing University, Nanjing 210046, China

[b]Department of Plant and Microbial Biology, University of California, Berkeley, California 94720

[c]The Key Laboratory of Western Resources Biology and Biological Technology, College of Life Sciences, Northwest University, Xi'an 710069, China

ORCID IDs: 0000-0001-8440-5571 (F.Zhang); 0000-0002-4906-9856 (F.Zhao); 0000-0002-2036-6443 (A.F.); 0000-0002-8375-8276 (S.L.); 0000-0002-9207-7915 (W.L.).

Plants cope with aluminum (Al) toxicity by secreting organic acids (OAs) into the apoplastic space, which is driven by proton (H^+) pumps. Here, we show that mutation of vacuolar H^+-translocating adenosine triphosphatase (H^+-ATPase) subunit a2 (VHA-a2) and VHA-a3 of the vacuolar H^+-ATPase enhances Al resistance in Arabidopsis (*Arabidopsis thaliana*). *vha-a2 vha-a3* mutant plants displayed less Al sensitivity with less Al accumulation in roots compared to wild-type plants when grown under excessive Al^{3+}. Interestingly, in response to Al^{3+} exposure, plants showed decreased vacuolar H^+ pump activity and reduced expression of *VHA-a2* and *VHA-a3*, which were accompanied by increased plasma membrane H^+ pump (PM H^+-ATPase) activity. Genetic analysis of plants with altered PM H^+-ATPase activity established a correlation between Al-induced increase in PM H^+-ATPase activity and enhanced Al resistance in *vha-a2 vha-a3* plants. We determined that external OAs, such as malate and citrate whose secretion is driven by PM H^+-ATPase, increased with PM H^+-ATPase activity upon Al stress. On the other hand, elevated secretion of malate and citrate in *vha-a2 vha-a3* root exudates appeared to be independent of OAs metabolism and tolerance of phosphate starvation but was likely related to impaired vacuolar sequestration. These results suggest that coordination of vacuolar H^+-ATPase and PM H^+-ATPase dictates the distribution of OAs into either the vacuolar lumen or the apoplastic space that, in turn, determines Al tolerance capacity in plants.

In acidic soils, phytotoxic levels of active aluminum (Al) are released from Al-containing minerals when the pH drops to 5 or lower (Kochian, 1995). These active Al forms, primarily Al^{3+}, can severely threaten root vitality and inhibit primary root elongation, thus limiting the acquisition of nutrient elements and water necessary for crop growth, which makes Al toxicity a major constraint for crop production in acid soils (Kochian, 1995; Ma, 2007). Such symptoms are generally recognized as the primary consequences from targeted actions of A1 in the root apex, specifically its distal part of the transition zone (DTZ). The DTZ, located between the apical meristem zone (MZ) and basal elongation zone, accumulates most of the Al contents in the root apex under Al stress and is the primary root site of Al toxicity (Ryan et al., 1993; Sivaguru and Horst, 1998).

Plants have evolved diverse adaptive strategies to cope with Al toxicity, among which external exclusion and internal tolerance are widely considered as the major mechanisms (Kochian, 1995; Ma, 2007). Both mechanisms are related to translocation of ions. For example, the exclusion mechanism is achieved by the secretion of organic acid (OA) anions, including malate, citrate, and oxalate, the specificities of which depend on the plant species, from the roots to externally chelate Al^{3+} (Miyasaka et al., 1991; Delhaize et al., 1993; Larsen et al., 1998; Zheng et al., 1998; Hoekenga et al., 2003, 2006; Sasaki et al., 2004). Furthermore, the tolerance mechanism underlies the sequestration of cytosolic Al^{3+} or its complex into the vacuoles (Vazquez et al., 1999; Shen et al., 2002; Illés et al., 2006). In Arabidopsis (*Arabidopsis thaliana*), malate and citrate are the major OAs in root exudates

[1]This work was supported by the National Natural Science Foundation of China (31770267) and the Program for Changjiang Scholars and Innovative Research Team in University from the Ministry of Education of China (IRT_14R27).

[2]Senior author.

[3]Author for contact: lanw@nju.edu.cn.

The author responsible for distribution of materials integral to the findings presented in this article in accordance with the policy described in the Instructions for Authors (www.plantphysiol.org) is: Wenzhi Lan (lanw@nju.edu.cn).

F.Zhang. and W.Z. conceived the original screening and research plans; W.Z. supervised the experiments; F.Zhang. performed most of the experiments with technical assistance from X.Y., X.H., M.L., Y.Y., and F.Zhao.; R.J., Y.-H.Y., and A.F. provided plant materials and analytic tools; F.Zhang. and W.Z. analyzed the data; W.Z. and S.L. conceived the project and wrote the article.

www.plantphysiol.org/cgi/doi/10.1104/pp.19.00626

under Al stress and are responsible for Al tolerance in Arabidopsis (Larsen et al., 1998; Hoekenga et al., 2003, 2006; Magalhaes et al., 2007; Liu et al., 2009). Intriguingly, although large amounts of cellular malate and citrate are originally stored in the vacuoles, considerable amounts are rapidly excreted through the PM-localized Al-activated malate transporter1 (ALMT1) and multidrug and toxic compound extrusion (MATE), respectively, after exposure to Al stress (Hoekenga et al., 2003, 2006; Kobayashi et al., 2007; Liu et al., 2009). Compared to the well-documented Al exclusion mechanism, the molecular mechanisms underlying vacuolar Al sequestration are poorly understood. Whereas several ATP-binding cassette–type transporters, including ALUMINUM SENSITIVE1 (ALS1), SENSITIVE TO ALUMINUM RHIZOTOXICITY1 (STAR1), and ALS3, have been suggested to be vital factors for Al tolerance in Arabidopsis (Larsen et al., 2005, 2007; Huang et al., 2010), the nature of these transporters remains elusive. Recent reports showed that ALS3 interacts with STAR1 to form an ATP-binding cassette transporter complex in the tonoplast and functions in phosphate (Pi) deprivation-induced root growth inhibition (Belal et al., 2015; Dong et al., 2017; Godon et al., 2019; Wang et al., 2019), suggesting that these transporters may have more functions in addition to coping with Al toxicity.

In plants, the active transport of ions is fundamentally driven by the proton (H^+) gradients established by H^+ pumps, namely, plasma membrane H^+-translocating adenosine triphosphatase (PM H^+-ATPase), vacuolar H^+-ATPase (V-ATPase), and vacuolar H^+-pyrophosphatase (V-PPase; Gaxiola et al., 2007; Schumacher and Krebs, 2010). The function of PM H^+-ATPase upon Al stress likely depends on plant species and genotypes. For example, the Al-induced activation of PM H^+-ATPase is found to coincide with secretion of OAs in soybean (*Glycine max*) roots (Shen et al., 2005; Liang et al., 2013), but PM H^+-ATPase in barley (*Hordeum vulgare*; Matsumoto, 1988) and summer squash (*Cucurbita pepo*) roots (Ahn et al., 2001) is inhibited by Al treatment. Consistent with the observations in soybean roots, PM H^+-ATPase is found to be activated by Al stress in Arabidopsis roots (Shen et al., 2005; Bose et al., 2010). The PM H^+-ATPase in Arabidopsis is encoded by 11 isoforms of P-type ATPases (AHA1–AHA11; Palmgren, 2001; Gaxiola et al., 2007). The *AHA* genes are differentially expressed in Arabidopsis tissues, and eight of them (*AHA1–AHA4*, *AHA7*, *AHA8*, *AHA10*, and *AHA11*) are expressed in roots (Ueno et al., 2005). Despite the fact that apoplastic acidification is generally observed upon Al stress (Zhang et al., 2017), little is known about how PM H^+-ATPase is linked to Al response in Arabidopsis. The PM H^+-ATPase activity has been hypothesized to be related to the activity of vacuolar H^+ pump (Li et al., 2005; Cho et al., 2012), which is constituted by V-ATPase and V-PPase (Gaxiola et al., 2007). In Arabidopsis, two tonoplast-localized isoforms of vacuolar H^+-ATPase subunit a (VHA-a), VHA-a2 and VHA-a3, provide the H^+-translocating activity. Compared to the wild type, *vha-a2 vha-a3* double mutant plants, in which the majority of V-ATPase activity is eliminated, display a retarded growth phenotype and are hypersensitive to excessive metals, including zinc (Zn) and calcium (Ca; Krebs et al., 2010; Tang et al., 2015). Another Arabidopsis vacuolar H^+ pump, Arabidopsis type-1 V-PPase (AVP1), is a major vacuolar H^+-pumping pyrophosphatase and has been shown to be involved in improving plant growth (Li et al., 2005; Ferjani et al., 2011; Segami et al., 2018). To ensure that plant cells respond appropriately to constantly changing environmental ions, the PM H^+-ATPase and vacuolar H^+ pumps may tightly coordinate to establish spatial H^+ gradients across plasma and vacuole membranes and thus maintain cellular homeostasis of ions, including OAs. However, the functional relationship among these H^+ pumps in Arabidopsis response to Al stress remains elusive, despite the fact that translocation of OAs has been established as a major event in tolerance of Al toxicity.

In this study, we report that V-ATPase, but not V-PPase, is a major vacuolar H^+ pump functioning in Arabidopsis root response to Al stress. In contrast to its positive role in internal detoxification of other metals, V-ATPase was repressed by excessive Al^{3+} and knockout of its members AHA-a2 and VHA-a3 caused Al resistance. We further identified the relationship between V-ATPase and other H^+ pumps and found that the PM H^+-ATPase was activated and contributed to Al resistance in *vha-a2 vha-a3* mutant. A detailed functional analysis showed that these two types of H^+ pump coordinated to drive OAs allocation through the PM-localized transporters into the root exudates for chelating external Al^{3+} in a low Pi-independent manner. Thus, this study uncovers a previously unrecognized mechanism underlying Al exclusion achieved by regulation of V-ATPase activity in Arabidopsis roots.

RESULTS

The *vha-a2 vha-a3* Mutant Is Resistant to Al^{3+} Stress

Previous studies showed that VHA-a2 and VHA-a3 redundantly confer resistance in Arabidopsis to excessive metals, such as Zn^{2+} and Ca^{2+}, but not magnesium (Mg^{2+}), through vacuolar sequestration (Krebs et al., 2010; Tang et al., 2015). Considering the importance of pH gradients across the tonoplast in metal transport into the vacuole (Schumacher and Krebs, 2010), we checked whether the *vha-a2 vha-a3* mutant showed altered sensitivity to several other metals including Al^{3+} and manganese (Mn^{2+}), whose uptake by plants could be enhanced under the acidic conditions (Kochian et al., 2004). We included Zn^{2+}, Ca^{2+}, and Mg^{2+} as positive and negative controls (Krebs et al., 2010; Tang et al., 2015) in this analysis. On one-sixth strength Murashige and Skoog agar medium with pH 4.3 and pH 5.8, no significant difference was observed between *vha-a2 vha-a3* and wild-type seedlings (Supplemental Fig. S1). Moreover, in the presence of toxic levels of Ca^{2+}, Mn^{2+},

Zn^{2+}, or Mg^{2+}, the growth of the wild type and *vha-a2 vha-a3* mutant was similar and was not affected by pH (4.3 or 5.8) of the medium (Supplemental Fig. S1). In the presence of 150 μM $AlCl_3$, however, the *vha-a2 vha-a3* mutant displayed a more resistant growth phenotype with longer primary roots and more biomass on pH 4.3 medium compared with the wild type, whereas this mutant displayed similar growth as the wild type on pH 5.8 medium regardless of $AlCl_3$ supplementation (Supplemental Fig. S1). These results demonstrate that disruption of VHA-a2 and VHA-a3 function enhances the resistance to Al^{3+}, instead of creating a more sensitive response as shown for other metals, probably in a pH-dependent manner.

Primary root growth inhibition is a typical symptom of Al toxicity in plants (Ryan et al., 1993; Sivaguru and Horst, 1998); therefore, we decided to examine the root growth phenotypes in the wild type and *vha-a2 vha-a3* mutant grown under Al stress. Supplementation of 250 μM $AlCl_3$ to pH 4.3 medium caused a 72% and 53% inhibition of primary root growth of the wild-type and *vha-a2 vha-a3* seedlings, respectively (Fig. 1, A and B). We also observed the root structure and found that the root-apex structure in the wild-type and *vha-a2 vha-a3* mutant roots was comparable when they grew under the normal conditions. Under 250 μM Al^{3+} treatment, the DTZ of the wild-type root apex displayed notable callose formation, a sensitive indicator of Al injury to roots (Wissemeir et al., 1987; Horst et al., 1997; Sivaguru and Horst, 1998), whereas the DTZ of the *vha-a2 vha-a3* mutant root apex produced much less callose (Fig. 1C), suggesting that *vha-a2 vha-a3* mutant roots are more tolerant to Al toxicity than roots of the wild type. We further examined the changes in root growth under various $AlCl_3$ concentrations and found that the longer primary roots in the *vha-a2 vha-a3* mutant were also observed under other $AlCl_3$ concentrations ranging from 150 to 300 μM (Fig. 1, A and B). Moreover, the *vha-a2 vha-a3* mutant displayed longer primary roots than the wild type when $AlCl_3$ was replaced with $(Al)_2(SO_4)_3$ with Al^{3+} concentration up to 300 μM (Supplemental Fig. S2), indicating that the resistance in the *vha-a2 vha-a3* mutant to Al salts was specifically attributable to Al^{3+} and not to their anions as counterions. In contrast to the Al resistance observed in the *vha-a2 vha-a3* mutant, both the *vha-a2* single mutant and the *vha-a3* single mutant displayed similar growth as the wild type when exposed to 250 μM $AlCl_3$ (Supplemental Fig. S3),

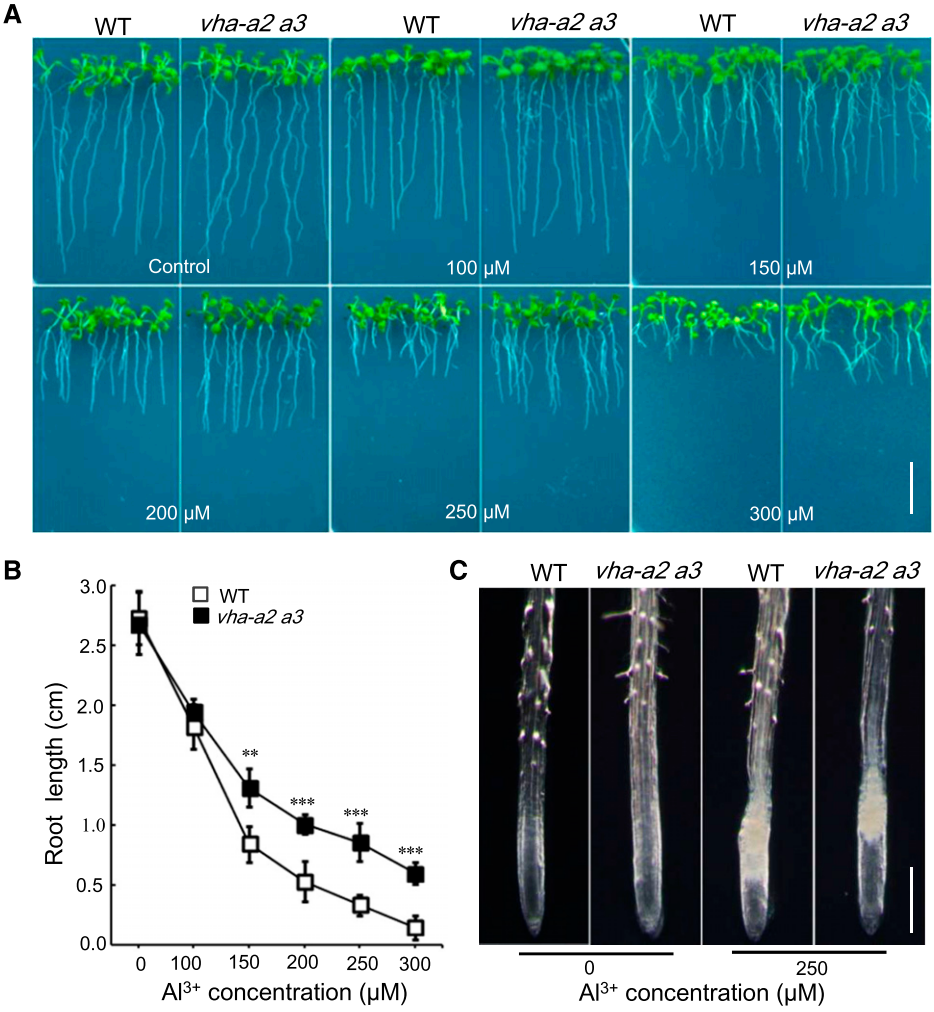

Figure 1. *vha-a2 vha-a3* mutant plants are resistant to external Al^{3+} in a dose-dependent manner. A and B, Growth phenotype (A) and length of primary roots (B) of 11-d-old wild-type (WT) and *vha-a2 vha-a3* mutant (*vha-a2 a3*) plants sown on medium supplemented with different concentrations of $AlCl_3$ as indicated compared to no treatment (control). Data are presented as the mean ± SD of four replicate experiments. Asterisks indicate statistically significant differences between the wild type and mutant plants (Student's *t* test; **, $P < 0.01$; ***, $P < 0.001$). C, Microscopy observation of 7-d-old root tips of wild type and *vha-a2 a3* plants grown on medium with or without 250 μM $AlCl_3$. Bars = 1 cm (A) and 100 μm (C).

indicating there is functional redundancy between VHA-a2 and VHA-a3 in response to Al^{3+} stress.

vha-a2 vha-a3 Mutant Roots Contain Less Al

To determine the mechanisms underlying Al resistance in the *vha-a2 vha-a3* mutant, we measured the Al content in wild-type and *vha-a2 vha-a3* plants using inductively coupled plasma-mass spectrometry (ICP-MS). After treatment with 250 μM Al^{3+} for 3 d, the Al content in the roots of both wild-type and mutant plants was strikingly elevated, and the Al elevation in the wild-type plants was remarkably higher than that in the mutant plants (Fig. 2A). In contrast to the considerable Al accumulation in roots, the Al content in shoots was not significantly altered, and both wild-type and *vha-a2 vha-a3* shoots displayed a similar Al content after treatment with 250 μM Al^{3+} (Fig. 2A). As Al is locally distributed in the root apex (Ryan et al., 1993; Sivaguru and Horst, 1998), we used hematoxylin, a dye shown to stain Al-rich deposits in Al-injured cell walls (Polle et al., 1978; Illés et al., 2006), to assist in the visualization of Al distribution in wild-type and *vha-a2 vha-a3* mutant root tips. After treatment with 150 μM Al^{3+} for 6 h, hematoxylin staining signals strongly expanded in the root-apex regions of the wild type, including the MZ and DTZ (Fig. 2B). By contrast, the signals in the *vha-a2 vha-a3* root apex were largely restricted at the DTZ, with much weaker signals in the remaining regions (Fig. 2B), indicating that the DTZ is still the target site of Al toxicity in *vha-a2 vha-a3* roots. We further used the fluorescence dye morin (2′,3′,4′,5,7-pentahydroxyflavone), which detects Al in the cytosol but neither cell wall bound Al nor vacuole-compartmentalized Al (Eggert, 1970; Larsen et al., 1998; Eticha et al., 2005), to examine internal Al accumulation. In the absence of Al^{3+}, the morin fluorescence signals were undetectable in wild-type and *vha-a2 vha-a3* mutant root apices (Fig. 2C). In the presence of 150 μM Al^{3+}, the signals abundantly appeared at the distal and proximal regions in the wild-type root apex and were stronger than those in the *vha-a2 vha-a3* mutant root apex (Fig. 2, C and D). Moreover, the DTZ in the *vha-a2 vha-a3* mutant displayed weaker fluorescence signals than the MZ (Fig. 2, C and D), which is opposite to the hematoxylin staining pattern (Fig. 2B), suggesting that there is differential distribution between external and internal Al. Taken together, these results demonstrate that the Al-resistant growth phenotype of the *vha-a2 vha-a3* mutant may be related to less Al accumulation in cell walls and inside the cells of the root apex, which are typical events in Al exclusion.

V-ATPase and V-PPase Activity Are Repressed upon Al Stress

The Al tolerance in the *vha-a2 vha-a3* mutant indicates a negative role of VHA-a2 and VHA-a3 in response to Al stress. To test how Arabidopsis plants regulate *VHA-a2* and *VHA-a3* under Al treatment, we analyzed the effect of Al stress on the expression of these two genes in wild-type roots. Time-course reverse transcription quantitative PCR (RT-qPCR) analysis showed that the levels of *VHA-a2* and *VHA-a3* transcripts decreased

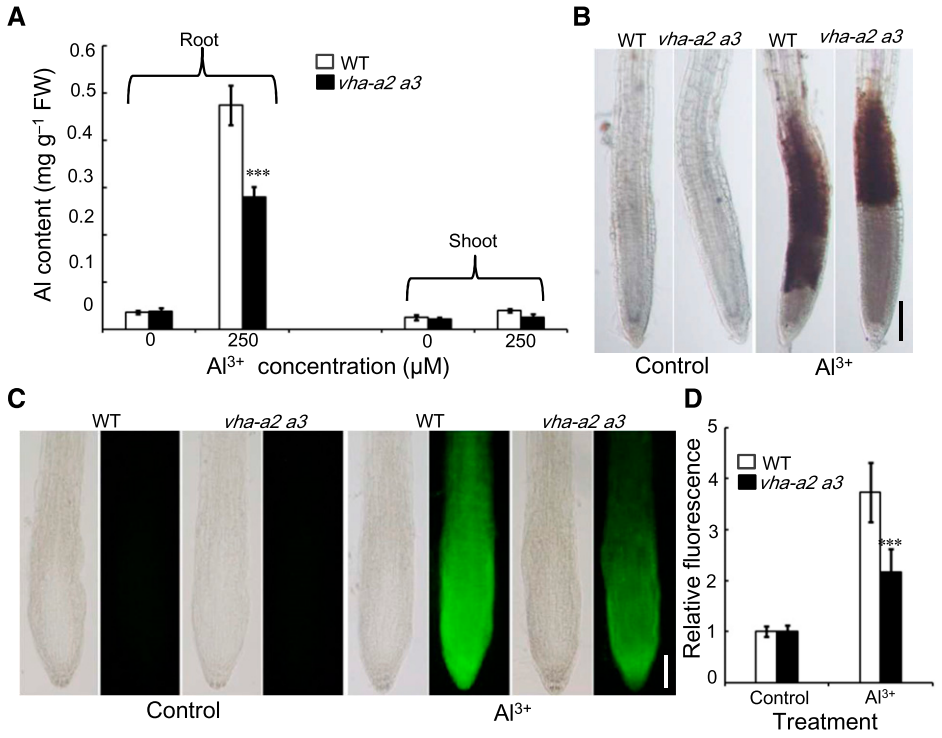

Figure 2. *vha-a2 vha-a3* mutant roots contain less Al after Al^{3+} treatment. A, Al contents in the root and shoot of the wild type (WT) and *vha-a2 vha-a3* mutant (*vha-a2 a3*) 3 d following transfer to the solutions with or without 250 μM Al^{3+}. FW, Fresh weight. B and C, Hematoxylin staining (B) and morin fluorescence signals (C) of root tips of 7-d-old wild type and *vha-a2 a3* mutant seedlings 6 h following treatment with 150 μM Al^{3+} (Al^{3+}) compared to no treatment (control). Bar = 50 μm (B) and 100 μm (C). D, Relative fluorescence intensity described in (C). Relative fluorescence level was normalized to wild type before Al^{3+} treatment as 1. Data in (A) and (D) are means ± SD from triple independent experiments. Asterisks represent a significant difference between the mutant lines and the wild type under the same culture conditions (Student's *t* test; ***, $P < 0.001$).

during the first 3 h after treatment and then remained at low levels (Fig. 3A). Remarkably, this down-regulation was specific to Al^{3+}, because other metals, such as Ca^{2+} and Zn^{2+}, rather up-regulated the expression level of *VHA-a2* and *VHA-a3* (Fig. 3B). Such changes in *VHA-a2* and *VHA-a3* transcript levels were parallel to the hypersensitive responses of the *vha-a2 vha-a3* mutant to these metals (Supplemental Fig. S1; Krebs et al., 2010; Tang et al., 2015). We further measured the V-ATPase activity in microsomal membranes isolated from wild-type and *vha-a2 vha-a3* mutant roots in the absence or presence of 250 μM Al^{3+}. In the absence of Al^{3+}, V-ATPase activity in the *vha-a2 vha-a3* mutant was 20% of that in the wild type (Fig. 3C), consistent with previous results (Krebs et al., 2010; Tang et al., 2012). After treatment with 250 μM Al^{3+} for 72 h, V-ATPase activity in the wild type was repressed by 20%, whereas that in the *vha-a2 vha-a3* mutant was unaffected (Fig. 3C). These results are consistent with the notion that VHA-a2 and VHA-a3 comprise the major V-ATPase activity, and they demonstrate that V-ATPase activity and its isoforms VHA-a2 and VHA-a3 are down-regulated under Al stress.

We also examined whether another vacuolar H^+ pump, namely, V-PPase, is affected by Al stress. Without Al treatment, V-PPase activity was comparable between wild-type and *vha-a2 vha-a3* root vacuoles (Fig. 3D), consistent with previous studies (Krebs et al., 2010; Tang et al., 2012). After treatment with 250 μM Al^{3+}, V-PPase activity in wild-type and *vha-a2 vha-a3* vacuoles was reduced by 22% and 53%, respectively (Fig. 3D). To examine a potential role of V-PPase activity in Al resistance, we isolated a transfer DNA insertion mutant of V-PPase *avp1-4* (GK-596F06-025557; Supplemental Fig. S4, A and B; Yang et al., 2018) and found that this mutant displayed a similar phenotype as the wild type when grown under 250 μM Al^{3+} (Supplemental Fig. S4, C and D). To test whether AVP1 contributes to Al resistance in the *vha-a2 vha-a3* mutant, we generated the *avp1-4 vha-a2 vha-a3* triple mutant by crossing the *avp1-4* mutant with the *vha-a2 vha-a3* mutant (Supplemental Fig. S4B) and found that the *avp1-4 vha-a2 vha-a3* triple mutant still displayed comparable growth to the *vha-a2 vha-a3* mutant in the absence or presence of 250 μM Al^{3+} (Supplemental Fig. S4, C and D). We also used *de-etiolated3* (*det3*) mutant, a vacuolar ATPase subunit C–defective mutant (Schumacher et al., 1999), and found that *det3* mutant exhibited a rate of Al-induced root growth inhibition comparable to that of the wild type (Supplemental Fig. S5). These results suggest that AVP1 and DET3 may not function in Al resistance in Arabidopsis plants.

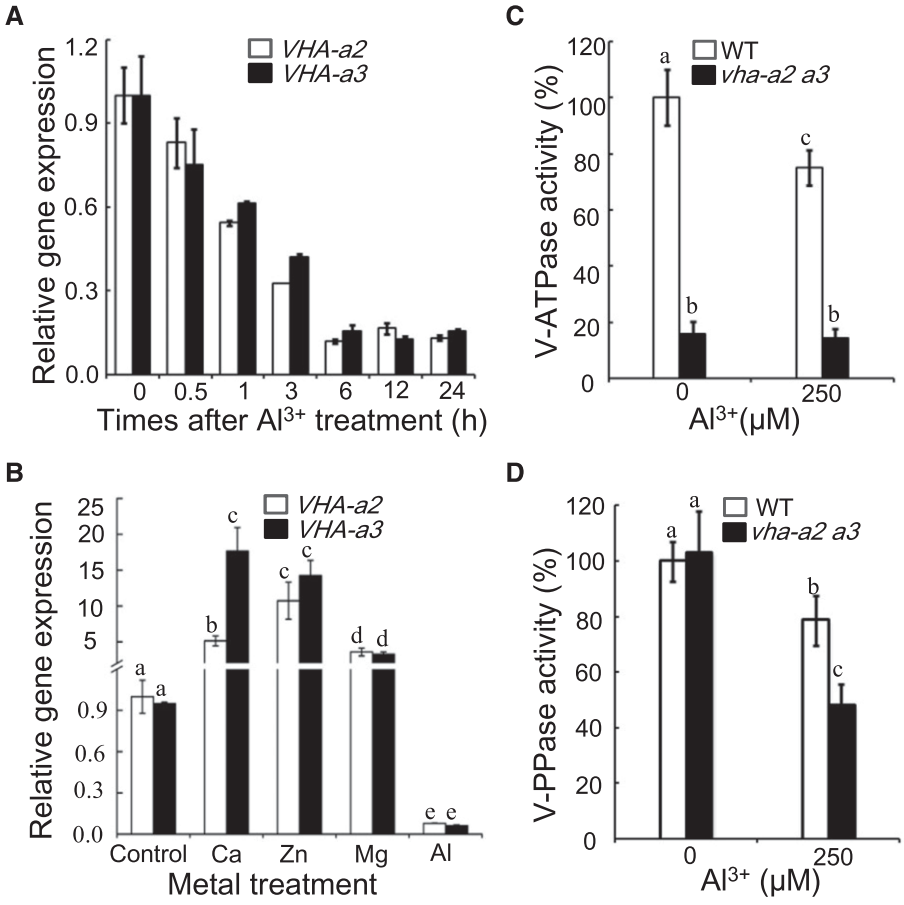

Figure 3. Vacuolar H^+ pumps are repressed by Al stress. A and B, RT-qPCR analysis of expression level of *VHA-a2* and *VHA-a3* genes in 2-week-old wild-type (WT) roots following various metal treatment. The time after which expression levels were measured is as indicated for 150 μM $AlCl_3$ treatment (A) and 12 h for 30 mM $CaCl_2$ (Ca), 0.4 mM $ZnCl_2$ (Zn), 10 mM $MgCl_2$ (Mg), and 150 μM $AlCl_3$ (Al) treatment (B). *ACTIN2* was used as an internal standard. Data are means ± SD. $n = 4$. C and D, V-ATPase (C) and V-PPase (D) activity in vacuolar membranes isolated from 5-week-old wild type and *vha-a2 vha-a3* mutant (*vha-a2 a3*) roots treated with 250 μM $AlCl_3$ treatment for 72 h (250) compared to no treatment (0). Data are shown as percentage of the wild type without Al^{3+} treatment. Data are means ± SD ($n = 3$). Values labeled with different letters are significantly different (Student's t test, $P < 0.05$).

The PM H$^+$-ATPase Is Activated and Contributes to Al Resistance in the *vha-a2 vha-a3* Mutant

As AVP1 and DET3 are unlikely to be responsible for Al resistance in the *vha-a2 vha-a3* mutant, we wondered whether other H^+ pumps, such as the one located at the PM, might serve as an alternative in this response. To this end, we initially examined H^+-ATPase activity in PM vesicles isolated from wild-type and *vha-a2 vha-a3* roots and found a similar activity in the vesicles from wild-type and *vha-a2 vha-a3* plants under control conditions. However, in the presence of 250 μM Al^{3+}, the H^+-ATPase in wild-type and *vha-a2 vha-a3* root PM vesicles was increased by ~20% and 40%, respectively (Fig. 4A), indicating that Al stress activates the PM H^+-ATPase particularly when V-ATPase is defective. In Arabidopsis roots, eight *AHA* genes (*AHA1*–*AHA4*, *AHA7*, *AHA8*, *AHA10*, and *AHA11*) were detected by RT-PCR assay (Ueno et al., 2005). We then analyzed the transcriptional level of these genes in wild-type and *vha-a2 vha-a3* roots treated without or with 150 μM Al^{3+}. Among these genes, the expression levels of *AHA1*, *AHA2*, and *AHA7* in wild-type roots were significantly up-regulated by Al treatment. Compared to that in the wild type, the expression levels of *AHA1*, *AHA2*, and *AHA7* in the *vha-a2 vha-a3* mutant were further increased by 1.6-, 5-, and 1.7-fold, respectively, and expression of the remaining genes was unaffected by Al treatment (Fig. 4B). Further time-course analysis showed that *AHA2* transcripts in wild-type and *vha-a2 vha-a3* roots were gradually up-regulated after exposure to Al stress, and the expression level in *vha-a2 vha-a3* roots was higher than that in wild-type roots after 3 h of the treatment (Fig. 4C). These results demonstrate that, in contrast to V-ATPase and V-PPase, PM H^+-ATPase activity is increased and could be further activated in *vha-a2 vha-a3* roots upon Al stress.

AHA2 is a major isoform of PM H^+-ATPase in Arabidopsis roots (Harper et al., 1990). Interestingly, we found that *AHA2* is the most responsive gene among *AHAs* to Al stress in the *vha-a2 vha-a3* root. We therefore used an *AHA2* mutation line, *aha2-4*, to evaluate the relationship between Al-induced activation of PM H^+-ATPase and Al resistance. The *aha2-4* mutant displayed a similar root growth phenotype as the wild type in

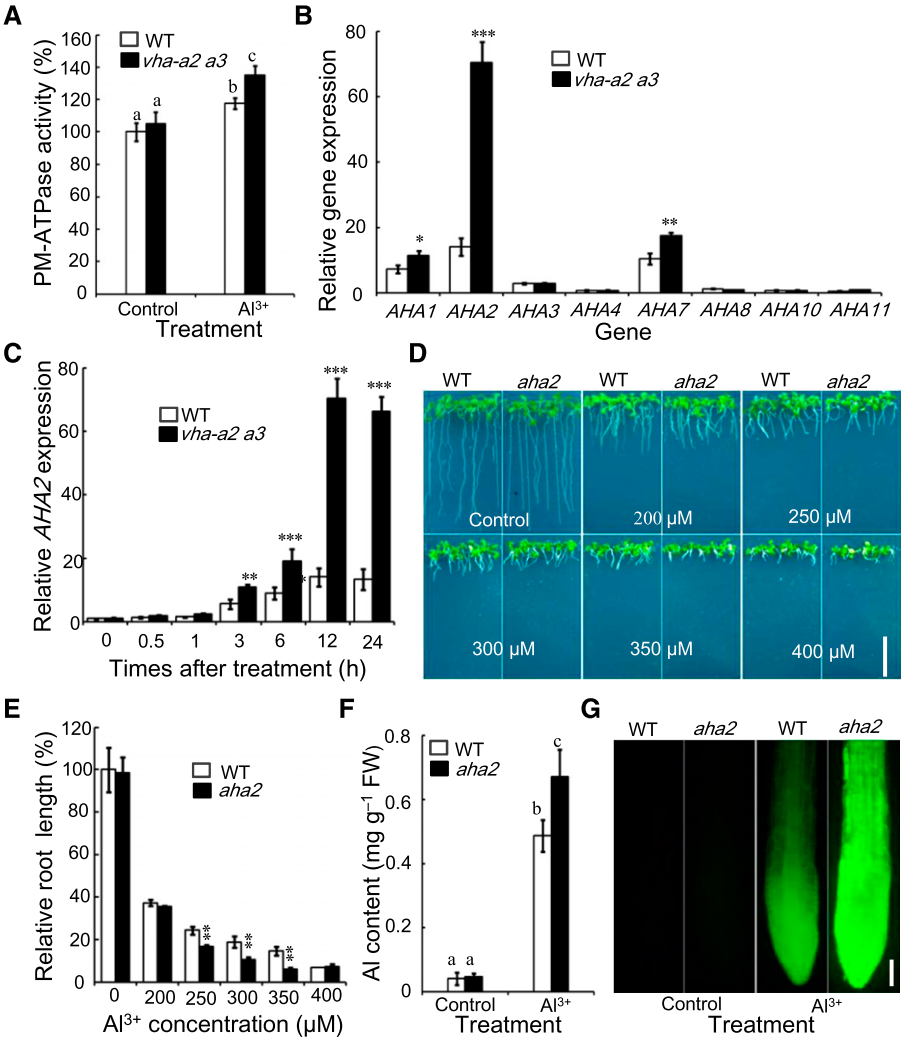

Figure 4. The PM H^+ pump contributes to the root response to Al stress. A, PM H^+ pump (PM-ATPase) activity in microsomal membranes isolated from 5-week-old wild-type (WT) and *vha-a2 vha-a3* mutant (*vha-a2 a3*) roots treated with 250 μM $AlCl_3$ for 72 h (Al^{3+}) compared to no treatment (control). B and C, Relative expression level of *AHAs* in 2-week-old wild type and *vha-a2 a3* roots at 12 h (B) or the times as indicated (C) after 150 μM $AlCl_3$ treatment. Expression levels were determined by RT-qPCR, and *ACTIN2* was used as an internal standard. Values in (A–C) are mean ± SD of three replicate experiments. D and E, Growth phenotype (D) and relative root length (E) of 11-d-old wild type and *aha2-4* seedlings treated with higher Al^{3+} concentrations. Relative root length in (E) was normalized to the wild type without Al^{3+} treatment as 100%. Data are means ± SD (n = 4). F, Al content in 5-week-old wild type and *aha2-4* roots treated with 250 μM $AlCl_3$ for 72 h (Al^{3+}) compared to no treatment (control). Data are means ± SD. n = 3. FW, Fresh weight. G, Morin fluorescence in 7-d-old wild type and *aha2-4* mutant root tips treated with 150 μM $AlCl_3$ for 6 h (Al^{3+}) or not (control). Bars = 1 cm (D) and 100 μm (G). Asterisks in (B), (C), and (E) indicate significant difference compared with the wild type (Student's t test; *, P< 0.05; **, P< 0.01; ***, P<0.001). Values labeled with different letters in (A) and (F) are significantly different (Student's t test, P < 0.05).

the control conditions. However, the *aha2-4* mutant displayed more severe growth retardation than the wild type under 250, 300, and 350 μM Al^{3+} treatment (Fig. 4, D and E). Moreover, ICP-MS analysis showed that *aha2-4* roots contained 28% more Al than wild-type roots after treatment with 250 μM Al^{3+} (Fig. 4F). Consistent with ICP-MS data, morin fluorescence signals in *aha2-4* roots were stronger compared to those in the wild type upon 150 μM Al^{3+} treatment (Fig. 4G), indicating that AHA2 contributes to Al resistance in Arabidopsis roots.

To validate the role of AHA2 in Al resistance in the *vha-a2 vha-a3* mutant, we constructed the *aha2-4 vha-a2 vha-a3* triple mutant by genetically crossing *aha2-4* with the *vha-a2 vha-a3* mutant and subsequently characterizing its phenotype in the presence of various Al^{3+} concentrations (Fig. 5, A and B). The wild-type, *vha-a2 vha-a3*, and *vha2-4 vha-a2 vha-a3* plants grew comparably on control medium. Under higher Al^{3+} conditions (250, 350, and 400 μM), the *vha2 vha-a2 vha-a3* triple mutant displayed shorter primary roots than the *vha-a2 vha-a3* mutant, indicating that AHA2 is involved in Al resistance in the *vha-a2 vha-a3* mutant. Notably, this triple mutant still had longer roots than the wild type under these treatments (Fig. 5, A and B), suggesting that

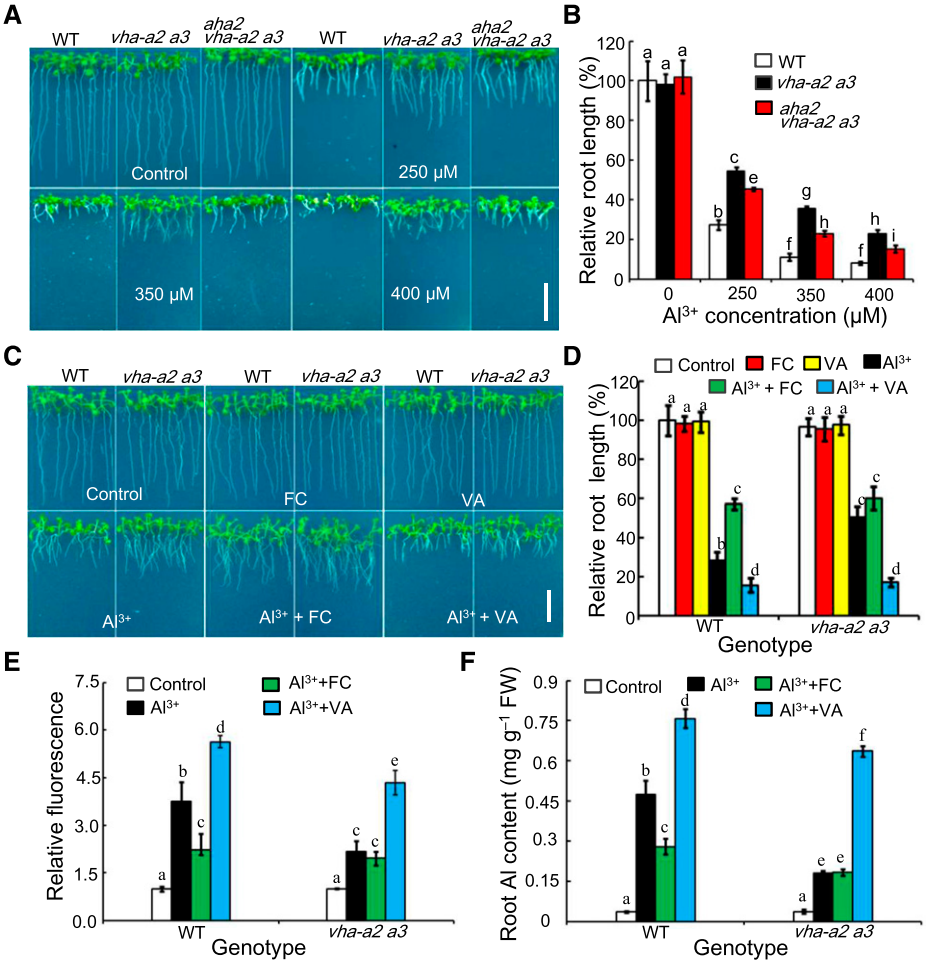

Figure 5. The PM H^+ pump is involved in the Al resistance in *vha-a2 vha-a3* mutant. A and B, Growth phenotype (A) and relative root length (B) of 11-d-old wild type (WT), *aha2-4*, *vha-a2 vha-a3* (*vha-a2 a3*), and *aha2-4 vha-a2 a3* triple mutant seedlings treated with higher Al^{3+} concentrations. C and D, Growth phenotype (C) and relative root length (D) of 11-d-old wild type and *vha-a2 a3* mutant seedlings grown under normal conditions (control) or treated with 250 μM $AlCl_3$ (Al^{3+}), 1 μM fusicoccin (FC), 5 μM vanadate (VA), 250 μM $AlCl_3$ and 1 μM FC (Al^{3+} + FC), or 250 μM $AlCl_3$ and 5 μM vanadate (Al^{3+} + VA). Relative root length in (B) and (D) was normalized to the wild type without Al^{3+} treatment set as 100%. Bars = 100 μm. Data are means ± SD of 15 independent plant samples in three replicates. E, Relative morin fluorescence intensity in the wild type and *vha-a2 a3* mutant root tips. After 6 h of 0 (control) or 150 μM $AlCl_3$ (Al^{3+}), 150 μM $AlCl_3$ and 1 μM FC (Al^{3+} + FC), or 150 μM $AlCl_3$ and 5 μM VA (Al^{3+} + VA) treatment, the 7-d-old plants were stained by morin for 6 h and roots were observed by microscopy. Relative fluorescence was normalized to the wild type without Al^{3+} treatment as 1. Data are mean ± SD. $n = 3$. F, Al content in 5-week-old wild type and *vha-a2 a3* roots at 72 h after treatment with 250 μM $AlCl_3$ (Al^{3+}), 250 μM $AlCl_3$ and 2 μM FC (Al^{3+} + FC), 250 μM $AlCl_3$ and 10 μM VA (Al^{3+} + VA), or no treatment (control). Data are means ± SD. $n = 4$. FW, Fresh weight. Values labeled with different letters are significantly different analyzed with two-way ANOVA (Tukey's HSD test, $P < 0.05$).

AHA2 is an important PM H^+-ATPase isoform in the maintenance of root Al resistance when V-ATPase is defective.

To further clarify whether PM H^+-ATPase is a critical linker to the achievement of Al resistance through defective V-ATPase, we applied a PM H^+-ATPase activator and inhibitor to examine their effects on root Al response of the wild type and the *vha-a2 vha-a3* mutant. As shown in Figure 5, C and D, addition of 1 μM fusicoccin, an activator of PM H^+-ATPase (Rasi-Caldogno et al., 1986; Shen et al., 2005; Zhu et al., 2005), rescued the Al-induced inhibition of wild-type root growth, creating a phenotype that was similar to that of the *vha-a2 vha-a3* mutant. On the other hand, addition of 5 μM vanadate, a PM H^+-ATPase inhibitor (Shen et al., 2005), inhibited the root growth of the *vha-a2 vha-a3* mutant and affected Al resistance of the *vha-a2 vha-a3* mutant, creating Al sensitivity as in the wild type (Fig. 5, C and D). Such changes in root growth were relevant to Al response, as both additions did not affect the growth phenotypes of the wild type and the *vha-a2 vha-a3* mutant in the absence of Al^{3+} (Fig. 5, C and D). We next examined Al accumulation in the wild-type and *vha-a2 vha-a3* mutant roots using fluorescence and ICP-MS analyses. The morin fluorescence analysis showed that 1 μM fusicoccin alleviated, whereas 5 μM vanadate enhanced, the fluorescence intensity, and both treatments consequently caused comparable levels of fluorescence in wild-type and *vha-a2 vha-a3* mutant roots upon Al stress (Fig. 5E). Consistent with the morin fluorescence analysis, ICP-MS analysis showed that 2 μM fusicoccin reduced Al content in the wild type by 41% (Fig. 5F). In addition, 10 μM vanadate increased Al content in wild-type and *vha-a2 vha-a3* mutant roots by 38% and 72%, respectively (Fig. 5F). These results further support the hypothesis that PM H^+-ATPase activity contributes to the defective V-ATPase–induced root Al resistance.

PM H^+-ATPase Contributes to H^+ and Malate Efflux under Al Stress

The PM H^+-ATPase mediates H^+ efflux into the apoplast (Gaxiola et al., 2007; Zhang et al., 2017). To examine whether PM-ATPase activity affects apoplastic pH in wild-type and *vha-a2 vha-a3* mutant roots during Al exposure, we measured the pH value in the nonbuffer solutions containing 250 μM Al^{3+} on which the wild type or the *vha-a2 vha-a3* mutant was grown, and we found that the *vha-a2 vha-a3* mutant caused a more significant pH decrease than the wild type after 3 h of incubation (Supplemental Fig. S6). Next, we used the fluorescent pH indicator 8-hydroxypyrene-1,3,6-trisulfonic acid trisodium salt (HPTS; Barbez et al., 2017) to measure the apoplastic pH. We immersed 7-d-old seedlings after treatment in one-sixth strength Murashige and Skoog solution containing HPTS with initial pH 5.0 for 30 min and selected two different channels with excitation wavelengths of 405 and 458 nm to visualize the protonated and deprotonated forms of HPTS, respectively (Fig. 6A). In the absence of Al^{3+}, the 458/405 ratios of the MZ epidermal cells in the wild-type and the *vha-a2 vha-a3* mutant root apex were 0.36 and 0.28, respectively (Fig. 6). In the presence of 150 μM Al^{3+}, the deprotonated HPTS signals (excitation, 458 nm) in wild-type and *vha-a2 vha-a3* mutant root apices became weaker (Fig. 6A). Moreover, the 458/405 ratios in wild-type and *vha-a2 vha-a3* mutant root apex were reduced to 0.24 and 0.15, respectively (Fig. 6, B and C), suggesting a higher apoplastic pH in the wild type. These results indicate that loss of VHA-a2 and VHA-a3 contributes to root-apex H^+ secretion under Al stress.

Given the enhanced H^+ efflux through activated PM H^+-ATPase is responsible for root Al resistance, lowered external pH might also enhance root growth as observed in the *vha-a2 vha-a3* mutant. To examine this possibility, we applied nonbuffered mediums with pH values of 4.3, 4.9, 5.5, and 5.8 and compared the growth phenotype of the wild type and the *vha-a2 vha-a3* mutant. Without Al^{3+} treatment, we observed similar root growth between the wild type and the *vha-a2 vha-a3* mutant under these acidic conditions (Supplemental Fig. S7, A–C). Moreover, in the presence of 250 μM Al^{3+}, the *vha-a2 vha-a3* mutant displayed similar responses to pH 4.3 or pH 4.9 (Supplemental Fig. S7, D–F). We also found that these pH values did not change the differential levels of Al-induced inhibition of root growth and biomass between the wild type and the *vha-a2 vha-a3* mutant (Supplemental Fig. S7, D–F), which is in agreement with the previous observations in bread wheat (*Triticum aestivum*; Pellet et al., 1997). We supplemented the medium with the pH buffer agent and found that growth, including biomass and primary root length, of the *vha-a2 vha-a3* mutant was still comparable to that of the wild type under pHs ranging from 4.3 to 5.8 (Supplemental Fig. S8). These results demonstrate that an increase in H^+ secretion did not mimic the enhanced Al resistance in the *vha-a2 vha-a3* mutant.

In Arabidopsis root Al response, the PM H^+-ATPase functionally bears the exudation of malate and citrate (Zhang et al., 2017), the major Al^{3+} chelators (Ma et al., 2001). The increase in apoplastic H^+ observed in the plants with defective V-ATPase may provide a stronger H^+ motive force across the PM, which could facilitate the efflux of cytosolic anions, including malate and citrate. We thus examined the malate and citrate content in wild-type and *vah-a2 vha-a3* root exudates using HPLC analysis (Supplemental Fig. S9). Without Al treatment, *vha-a2 vha-a3* roots released a little more malate and citrate than wild-type roots (Fig. 7, A and C). After exposed to 250 μM Al^{3+}, however, *vha-a2 vha-a3* roots secreted more malate and citrate (1.8- and 1.6-fold, respectively) than the wild-type roots (Fig. 7, A and C). To verify the correlation of these OAs exudation with the PM H^+-ATPase activity, we supplemented with the PM H^+-ATPase inhibitor vanadate and found that 10 μM vanadate treatment inhibited malate and citrate content in *vha-a2 vha-a3* root exudates by 70% and 53%, respectively, and diminished

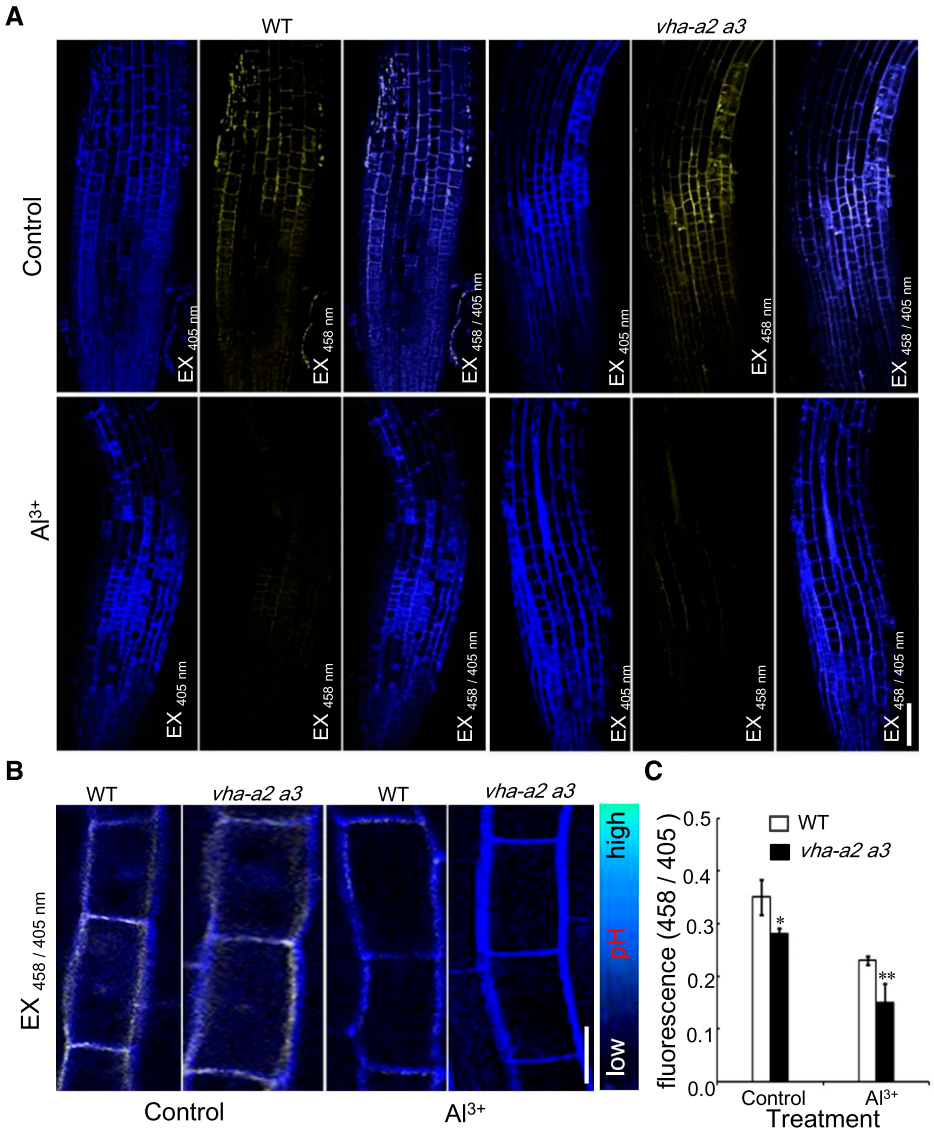

Figure 6. Apoplastic acidification of Arabidopsis roots upon Al stress. A, Root-apex HPTS fluorescence signals in 7-d-old wild-type (WT) and *vha-a2 vha-a3* (*vha-a2 a3*) mutant seedlings treated with 150 μM Al^{3+} (Al^{3+}) or not (control). The root-apex fluorescent signals represented protonated HPTS (EX405; excitation, 405 nm; emission peak, 514 nm), deprotonated HPTS form (EX458; excitation, 458 nm; emission peak, 514 nm), and the ratio of EX405 to EX458 (EX405/EX458). B and C, Representative images of the MZ cortex cells (B) and summarized values (C) on fluorescent ratio of protonated HPTS to deprotonated HPTS in the MZ cortex cells of wild type and *vha-a2 a3* mutant roots. Color code (black to green) depicts (low to high) 458/405 intensity. Bars = 60 μm (A) and 200 μm (B). Data are mean ± SD ($n = 3$) and were calculated from 20 cells in three roots. Asterisks indicate statistically significant differences compared with wild type (Student's *t* test; *, $P < 0.05$; **, $P < 0.01$).

the different degrees in these OAs contents between wild-type and *vha-a2 vha-a3* roots under Al stress (Fig. 7, A and C), suggesting that the activation of PM H^+-ATPase activity contributes to the increase in root OAs excretion upon Al stress.

We further examined whether this root OAs excretion is involved in Al resistance in the *vha-a2 vha-a3* mutant using exogenous application of malate and citrate. Although 10 μM malate and 20 μM citrate did not affect the normal growth of the wild type and the *vha-a2 vha-a3* mutant, they rescued Al-induced primary root growth inhibition in the wild type by 30% and 23% (Fig. 7, E and F). In addition, the root growth of the wild type was similar to that of the *vha-2 vha-a3* mutant under these treatments (Fig. 7, E and F). We also used OAs transport inhibitors niflumic acid (NIF) and anthracene-9-carboxylic acid (9-AC), which have been found to efficiently inhibit Al-induced root malate and citrate exudation (Osawa and Matsumoto, 2002; Zhu et al., 2005; Wang et al., 2007), on the wild type and *vha-a2 vha-a3* mutant. Under control conditions, 0.1 μM NIF and 0.2 μM 9-AC did not significantly affect the growth of the wild type and the *vha-a2 vha-a3* mutant. When combined with 250 μM Al^{3+}, however, both inhibitors diminished the Al-resistant growth of the *vha-a2 vha-a3* mutant, resulting in comparable root length between the wild type and the *vha-a2 vha-a3* mutant (Fig. 7, E and F). Together, these results indicate that the increases in OAs levels released from *vha-a2 vha-a3* roots contribute to the enhanced Al resistance of the *vha-a2 vha-a3* mutant.

Defective V-ATPase–induced Al Resistance Is Independent of OA Synthesis and Tonoplast-Localized ALS3 and STAR1

To determine whether the increases in malate and citrate in *vha-a2 vha-a3* root extrudes come from Al-induced OAs synthesis, we examined the RNA levels of malate

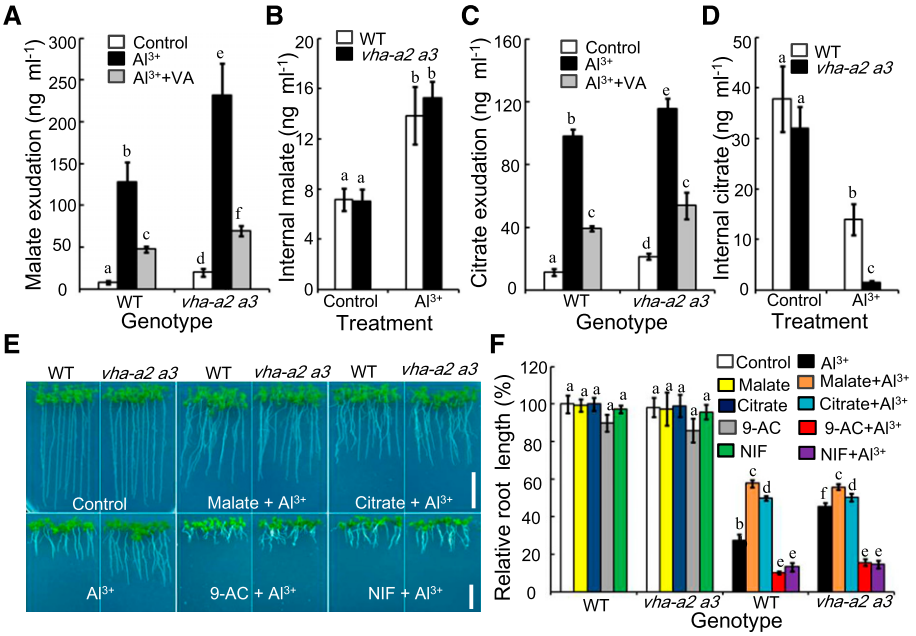

Figure 7. Al stress redistributes malate and citrate for Al resistance. A and C, Malate (A) and citrate exudation (C) from 5-week-old wild-type (WT) and *vha-a2 vha-a3* mutant (*vha-a2 a3*) plants incubated in normal solutions (control) or in solutions containing 250 μM $AlCl_3$ (Al^{3+}) or 250 μM $AlCl_3$ and 20 μM vanadate (Al^{3+} + VA) for 72 h. Data are mean ± SD ($n = 3$). B and D, Malate (B) and citrate content (D) in 5-week-old wild type and *vha-a2 a3* roots incubated in solutions without (control) or with 250 μM $AlCl_3$ (Al^{3+}) for 72 h. Data are mean ± SD ($n = 3$). E and F, Growth phenotype (E) and relative root length (F) of 11-d-old wild type and *vha-a2 a3* seedlings grown under normal conditions (control) or experimental conditions supplemented with 10 μM malate (malate), 20 μM citrate (citrate), 250 μM $AlCl_3$ (Al^{3+}), 10 μM malate and 250 μM Al^{3+} (malate + Al^{3+}), 20 μM citrate and 250 μM Al^{3+} (citrate + Al^{3+}), 0.1 μM NIF, 0.2 μM 9-AC, 250 μM Al^{3+} and 0.1 μM NIF (NIF + Al^{3+}), or 250 μM Al^{3+} and 0.2 μM 9-AC (9-AC + Al^{3+}). Bars = 1 cm. Relative root length was normalized to the wild type without Al^{3+} treatment set as 100%. Data are means ± SD of three independent plant samples in three replicates. Values in (A–D) and in (F) labeled with different letters are significantly different analyzed with one-way ANOVA (Student's *t* test, $P < 0.05$) and two-way ANOVA (Tukey's HSD test, $P < 0.05$), respectively.

and citrate metabolism genes, including peroxisomal NAD-malate dehydrogenase1 (*PMDH1*), mitochondrial malate dehydrogenase1 (*MMDH1*), *MMDH2*, malate dehydrogenase1 (*MDH1*), citrate synthase1 (*CSY1*), and *CSY3* in the wild type and the *vha-a2 vha-a3* mutant. RT-qPCR analysis showed that although the transcription levels of most genes, including *PMDH1*, *MMDH1*, *MMDH2*, *CSY1*, and *CSY3*, but not *MDH1*, were up-regulated, their levels were comparable between wild-type and *vha-a2 vha-a3* roots after Al stress (Supplemental Fig. S10). These results suggest that further increases in OAs within *vha-a2 vha-a3* root extrude are independent of Al-induced capacities of malate and citrate synthesis, consistent with previous results obtained from Al-sensitive and Al-resistant triticale genotypes (Hayes and Ma, 2003).

In mature plant cells, the vacuoles occupy as much as 90% of the cellular volume and contain the major proportions of malate and citrate (Marty, 1999; Meyer et al., 2010). A defect in V-ATPase may impair vacuolar malate and citrate sequestration, because this process requires a well-established H^+ gradient across the tonoplast (Sze et al., 1999; Schumacher and Krebs, 2010; Seidel et al., 2013). To check this hypothesis, we measured internal malate and citrate content in the wild type and the *vha-a2 vha-a3* mutant without or with 250 μM Al^{3+} treatment. The wild type and the *vha-a2 vha-a3* mutant had similar content of basal malate and citrate without Al^{3+} treatment. In the presence of Al^{3+}, however, the *vha-a2 vha-a3* mutant contained a similar malate content and less citrate content compared to that in the wild type after Al^{3+} exposure (Fig. 7, B and D), implying that vacuolar OAs storage is impaired in the *vha-a2 vha-a3* mutant. To test this idea, we examined the expression patterns of *ALS3* and *STAR1*, two important tonoplast-localized transporters that function in Al tolerance (Larsen et al., 1998, 2005; Huang et al., 2010; Dong et al., 2017; Wang et al., 2019), and we found that neither of these had significantly different transcriptional levels between the wild type and the *vha-a2 vha-a3* mutant upon Al treatment (Supplemental Fig. S11, B and C). To further examine the role of ALS3 and STAR1, we performed genetic analysis of *als3* and *star1* mutant plants with defective V-ATPase activity induced by concanamycin A (ConcA), a V-ATPase activity inhibitor (Supplemental Fig. S11; Gaxiola et al., 2007). Under control growth conditions, the wild type and *als3* and *star1* mutants grew similarly and were not affected by

the addition of 5 nM ConcA. As reported previously by Larsen et al., 2005, 2007; Huang et al., 2010, primary root growth in *als3* and *star1* mutant plants was more severely inhibited by 250 Al^{3+} μM compared to in the wild type. However, Al-induced inhibition of primary root growth of the wild type, *als3*, and *star1* was rescued by ConcA applied at a similar level by ~40% (Supplemental Fig. S11, D and E). Therefore, these data not only confirm the notion that a defect in V-ATPase contributes to Al resistance but also demonstrate that ALS3 and STAR1 are not involved in Al resistance related to V-ATPase activity.

PM-Localized ALMT1 Is Activated to Mediate Al Resistance Caused by Defective V-ATPase

The finding of elevated secretion of malate and citrate in *vha-a2 vha-a3* mutant root exudates suggests a connection between the PM-localized transporters, namely, malate transporter ALMT1 and citrate transporter MATE, and Al resistance in the *vha-a2 vha-a3* mutant. We therefore assessed the expression patterns of *ALMT1* and *MATE* genes under Al stress and found that these two genes in wild-type roots were significantly up-regulated in a time-dependent manner after exposure to 250 μM Al^{3+} (Fig. 8A; Supplemental Fig. S11A). The up-regulation of *ALMT1* expression was further elevated in *vha-a2 vha-a3* mutant roots (Fig. 8A). We also analyzed the transcript levels of Sensitive to Proton Rhizotoxicity1 (*STOP1*) and WRKY (amino acid sequences)-type transcription factor *WRKY46*, two well-characterized transcription factors that up- and down-regulate *ALMT1* gene expression, respectively (Iuchi et al., 2007; Ding et al., 2013). We found that the *vha-a2 vha-a3* mutant had a higher transcript level of *STOP1* and a lower transcript level of *WRKY46* than that in the wild type under Al stress (Fig. 8, B and C), findings that are consistent with the higher level of *ALMT1* in the *vha-a2 vha-a3* mutant compared with that in the wild type.

We next evaluated whether ALMT1 contributes to the Al resistance caused by defective V-ATPase by using the *ALMT1* insertional knockout mutant line *almt1* (SALK_00962). As reported previously (Hoekenga et al., 2006), *almt1* displayed a hypersensitive root growth with 250 μM Al^{3+} treatment compared with the wild type (Fig. 8, D and E). Accordingly, Al-induced morin fluorescence signals in *almt1* mutant root tips were stronger than those in wild-type root tips (Fig. 8, F and G). We then examined the effect of ConcA on wild-type and *almt1* mutant responses to Al stress. We found that 5 nM ConcA rescued root growth inhibition by 40% and reduced the morin fluorescence signals by 32% in the wild type treated with 250 μM Al^{3+} (Fig. 8, D–G). In contrast with the changes in the wild type, the Al-induced root growth inhibition and morin fluorescence signals in *almt1* mutant root tips were only slightly affected by the ConcA treatment (Fig. 8, D–G), implying that ALMT1 is an important transporter required for defective V-ATPase–induced Al resistance.

Disturbance of Malate Efflux across the PM Overrides Al-Inhibited Expression of *VHA-a2* and *VHA-a3*

Cytosolic OAs may be secreted into either the apoplastic space or the vacuole lumen. Our finding that the Al-induced suppressed V-ATPase activity activated ALMT1 led us to explore what may happen to V-ATPase activity when OAs efflux through the PM is impaired. To this end, we added 9-AC or vanadate, which inhibits OAs exudation from the roots (Fig. 7; Zhu et al., 2005; Wang et al., 2007) and diminishes the Al resistance in the *vha-a2 vha-a3* mutant (Fig. 7), to the experimental treatment without or with 250 μM Al^{3+}. As shown in Figure 9A, addition of 0.2 μM 9-AC or 5 μM vanadate alone weakly increased the levels of *VHA-a2* and *VHA-a3* transcript. When combined with 250 μM Al^{3+}; however, addition of 9-AC overrode the Al-induced inhibition of transcript levels of both *VHA-a2* and *VHA-a3*, which were dramatically up-regulated more than 10-fold compared with their expression levels under Al^{3+} or 9-AC treatment (Fig. 9A). In addition, such an override also occurred in the presence of 5 μM vanadate but to a much lesser extent (Fig. 9A). On the other hand, addition of 0.2 μM 9-AC or 5 μM vanadate severely reduced Al-induced up-regulation of *ALMT1* expression (Fig. 9C). To further investigate the relationship between these Al-induced changes, we examined whether the ALMT1 mutation affects the expression patterns of *VHA-a2* and *VHA-a* and found that both *VHA-a2* and *VHA-a3* transcripts were expressed at similar levels in the wild type and *almt1* mutant without Al^{3+} treatment. However, the transcript levels of both genes in the *almt1* mutant were much higher than those in the wild type after exposure to 250 μM Al^{3+} (Fig. 9B). Together, these results suggest that this Al-induced stimulation of V-ATPase activity may operate as a backup mechanism if the external Al exclusion is lost, which in turn enhances OAs or Al-OA complexes storage in the vacuoles, leading to internal Al tolerance.

Tolerance of Low Pi or Iron Toxicity Is Unlikely to Contribute to the Al Resistance in the *vha-a2 vha-a3* Mutant

High concentrations of Al^{3+} in the external medium may cause phosphorus deficiency, which subsequently inhibits primary root growth (Kochian et al., 2004). We thus assessed whether the Al resistance in the *vha-a2 vha-a3* mutant is related to a tolerance of low Pi stress. We first measured Pi content in wild-type and *vha-a2 vha-a3* mutant plants using ICP-MS analysis and found no difference in the Pi content of roots and shoots of both plants grown under conditions without or with 250 μM Al^{3+} (Supplemental Fig. S12A). Notably, addition of Al^{3+} slightly increased Pi content in roots but did not significantly affect Pi content in shoots (Supplemental Fig. S12A). Together, these results suggest that enhanced Al resistance in the *vha-a2 vha-a3* mutant is unlikely to be

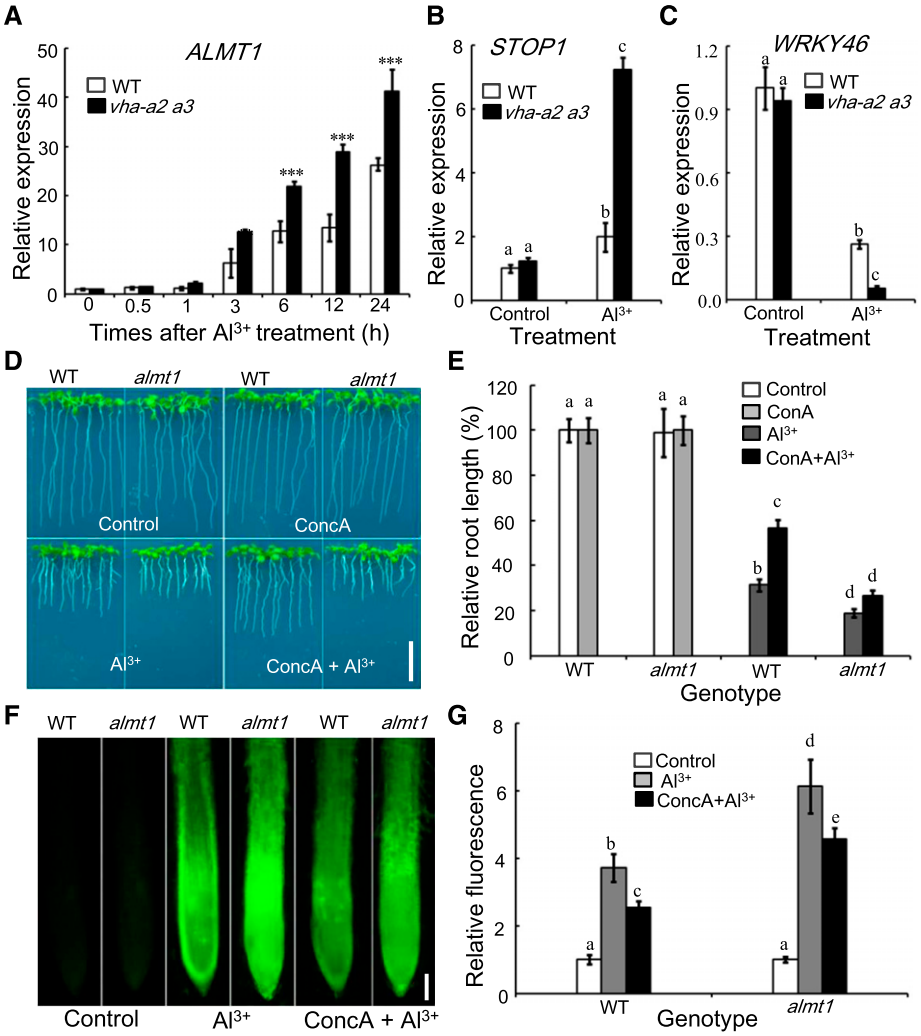

Figure 8. Defective V-ATPase activates a malate efflux system responsible for Al resistance. A to C, RT-qPCR assay of *ALMT1* (A), *STOP1* (B), and *WRKY46* (C) transcripts in roots of 2-week-old wild-type (WT) and *vha-a2 vha-a3* mutant (*vha-a2 a3*) plants following Al^{3+} treatment for the times as indicated in (A) or for 12 h (B and C). *ACTIN2* was used as the internal reference gene. D and E, Growth phenotype (D) and relative root length (E) of 11-d-old wild type and *almt1* mutant plants grown under normal conditions (control) or with 5 nM ConcA, 250 μM Al^{3+} (Al^{3+}), or 5 nM ConcA and 250 μM Al^{3+} (ConcA + Al^{3+}). F and G, Morin fluorescence signal (F) and relative fluorescence intensity (G) in 7-d-old wild type and *almt1* mutant root tips incubated in solutions without (control) or with 150 μM $AlCl_3$ (Al^{3+}) or 5 nM ConcA and 150 μM Al^{3+} (ConcA + Al^{3+}) for 6 h. Relative fluorescence was normalized to the wild type without Al^{3+} treatment set as 1. Data in (A–C) and (D) are mean ± SD ($n = 3$). Bars = 1 cm (D) and 50 μm (F). Relative root length in (E) was normalized to wild type without Al^{3+} treatment set as 1, and data are means ± SD of three independent plant samples in three replicates. Asterisks in (A) indicate statistically significant differences compared with the wild type (Student's *t* test; ***, $P < 0.001$), and values labeled with different letters in (B), (C), and (G) are significantly different (Student's *t* test, $P < 0.05$). Values labeled with different letters in (E) are significantly different analyzed with two-way ANOVA (Tukey's HSD test, $P < 0.05$).

a result of changes in low-Pi stress tolerance. To evaluate this possibility, we analyzed the expression patterns of genes involved in low-Pi resistance, including *LOW PHOSPHATE ROOT1* (*LPR1*), *NITROGEN LIMITATION ADAPTATION* (*NLA*), *PHOSPHATE1* (*PHO1*), *PHOSPHATE TRANSPORTER1;1* (*PHT1;1*), *PHT1;4*, and transcription factor *WRKY45* (Shin et al., 2004; Stefanovic et al., 2007; Svistoonoff et al., 2007; Lin et al., 2013; Wang et al., 2014). RT-qPCR data indicated that the expression levels of most of the tested genes were similar in the wild type and *vha-a2 vha-a3* roots under 250 μM Al^{3+} treatment, except for *PHT1;4* (Supplemental Fig. S12B), suggesting a comparable Pi response between the wild type and the *vha-a2 vha-a3* mutant. To examine whether Al resistance in the *vha-a2 vha-a3* mutant depends on Pi doses, we performed phenotypic analysis of the wild type and *vha-a2 vha-a3* mutant grown under conditions of 250 μM Al^{3+} with various Pi levels (Supplemental Fig. S12, C and D). On medium with a high, normal, and low level of Pi (2 mM, 200 μM, and 20 μM, respectively), *vha-a2*

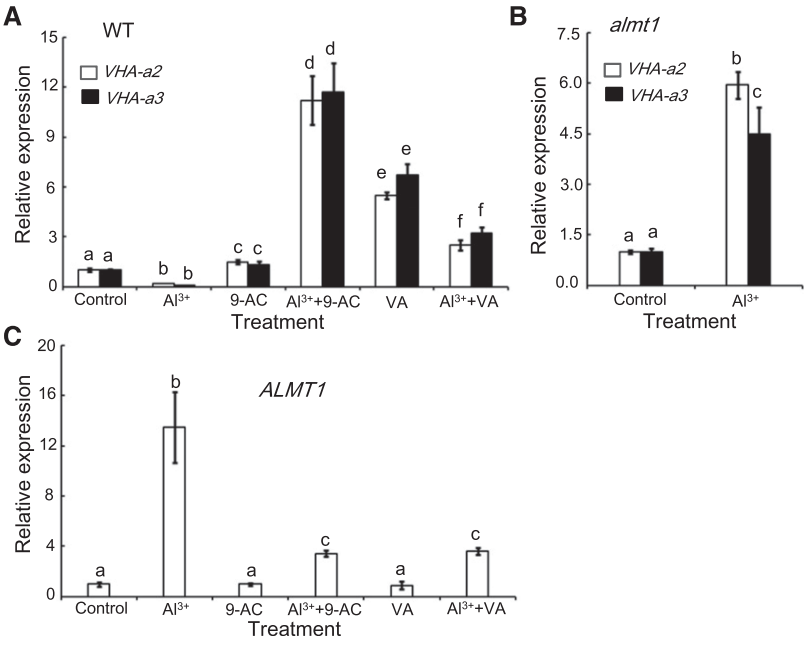

Figure 9. The impaired efflux of cytosolic OAs into apoplastic space regulates the expression of *VHA-a2*, *VHA-a3*, and *ALMT1*. A and C, RT-qPCR assay of *VHA-a2* and *VHA-a3* transcripts (A) and *ALMT1* transcripts (C) in roots of 2-week-old wild-type (WT) plants at 12 h after treatment with 150 μM $AlCl_3$ (Al^{3+}), 0.2 μM 9-AC, 150 μM $AlCl_3$ and 0.2 μM 9-AC (Al^{3+} + 9-AC), 5 μM vanadate (VA), and 150 μM Al^{3+} and 5 μM vanadate (Al^{3+} + VA) compared to no treatment (control). B, RT-qPCR assay of *VHA-a2* and *VHA-a3* transcripts in *almt1* roots (B) at 12 h after treatment with 150 μM $AlCl_3$ (Al^{3+}) compared to no treatment (control). *ACTIN2* was used as an internal standard. Values are mean ± SD of three replicate experiments, and values labeled with different letters in (A) or in (B) and (C) are significantly different analyzed with two-way ANOVA (Tukey's HSD test, $P < 0.05$) or one-way ANOVA (Student's *t* test, $P < 0.05$), respectively.

vha-a3 mutant and wild-type plants grew similarly. When combined with 250 μM Al^{3+}, these Pi levels did not abolish the *vha-a2 vha-a3* mutant phenotype of longer primary root compared to the wild type, further supporting our earlier hypothesis that enhanced Al resistance in the *vha-a2 vha-a3* mutant is not dependent on tolerance of Pi deficiency.

The over-accumulation of iron (Fe) in root is a critical factor in Pi deficiency-induced inhibition of primary root growth (Ward et al., 2008; Müller et al., 2015; Balzergue et al., 2017; Dong et al., 2017; Mora-Macías et al., 2017; Godon et al., 2019; Wang et al., 2019). To determine whether Al resistance in the *vha-a2 vha-a3* mutant may rather result from a tolerance of Fe toxicity, we measured the Fe content and analyzed Fe accumulation patterns in wild-type and *vha-a2 vha-a3* mutant roots. Similar to results reported previously by Tang et al. (2012), our ICP-MS data showed that Fe content in *vha-a2 vha-a3* roots was less than that in the wild type under normal conditions. However, in the presence of 250 μM Al^{3+}, the Fe content in the *vha-a2 vha-a3* mutant was nearly 40% higher than that in the wild type (Supplemental Fig. S13 A). Such changes appear to exclude the possibility that enhanced Al resistance in the *vha-a2 vha-a3* mutant results from internal high-Fe tolerance. Moreover, the staining patterns detected by Perls/diaminobenzidine staining method, which stains Fe^{2+} and Fe^{3+} accumulation in the root (Roschzttardtz et al., 2009; Dong et al., 2017), were similar between wild-type and *vha-a2 vha-a3* root tips treated without or with 250 μM Al^{3+} (Supplemental Fig. S13 B), indicating similar extracellular Fe distribution in roots of the two genotypes. Although the exact role of changes in Fe accumulation needs further clarification, these results demonstrate that the Al-resistance growth phenotype of *vha-a2 vha-a3* does not result from a tolerance of Fe stress.

DISCUSSION

Vacuoles are the main storage site for the majority of cellular ions and metabolites and are crucial for detoxification and nutrient homeostasis (Marty, 1999; Schumacher and Krebs, 2010). Vacuoles utilize the H^+ electrochemical gradient across the tonoplast energized by vacuolar H^+ pumps to regulate ions distribution (Sze et al., 1999). A defect in V-ATPase activity induced by VHA-a2 and VHA-a3 mutation causes a severely stunted growth phenotype, which largely results from impaired nutrient homeostasis crucial for plant development, including essential metal mineral nutrients, such as K^+, Ca^{2+}, and Zn^{2+} (Krebs et al., 2010; Tang et al., 2012). In this study, we found that, upon excessive Al^{3+}, the *vha-a2 vha-a3* mutant displayed an Al-resistance growth phenotype with longer primary roots, whereas *vha-a2* and *vha-a3* single mutants did not show discernible difference in Al resistance compared to wild-type plants (Fig. 1; Supplemental Fig. S1). Such phenotypes were only observed in the *vha-a2 vha-a3* mutant, whereas defects in other vacuolar H^+ pumps in Arabidopsis plants, including *avp1-4* and *det3* mutants, resulted in similar Al sensitivity as the wild type (Supplemental Figs. S4 and S5). Moreover, although V-PPase activity was reduced by Al stress when combined with defective V-ATPase (Fig. 3D), we found that V-PPase is not responsible for the Al resistance in the *vha-a2 vha-a3* mutant, because AVP1 mutation did not alter *vha-a2 vha-a3* mutant responses to Al^{3+} stress (Supplemental Fig. S4). We thus conclude that VHA-a2 and VHA-a3 are the dominant vacuolar H^+ pump subunits and function redundantly in mediating Al-induced inhibition of primary root growth. Consistent with the notion that V-ATPase functions in the vacuolar sequestration of metals (Krebs et al., 2010; Tang et al., 2012), our results also showed that the *vha-a2 vha-a3*

mutant had less Al content in roots and similar Al content in shoots compared with that of the wild type following exposure to Al stress. Moreover, *vha-a2 vha-a3* mutant roots accumulated less Al, including a decrease in cytosol Al content and reduced Al distribution in the cell wall of the root-apex MZ part (Fig. 2). Our results thus reveal that the Al-resistance growth phenotype of the *vha-a2 vha-a3* mutant is unlikely achieved by internal Al tolerance.

Several findings in this study support that Al resistance induced by defective V-ATPase is related to Al exclusion, which is mainly achieved by the secretion of OAs from roots to chelate external Al (Kochian, 1995; Ma, 2007). First, malate and citrate are major and moderate contributors, respectively, in Arabidopsis root exudates for detoxifying external Al^{3+} (Liu et al., 2009; Meyer et al., 2010). We found these two OAs were considerably released upon Al stress particularly when V-ATPase was defective (Fig. 7), suggesting that Arabidopsis fine tunes the function of VHA-a2 and VHA-a3 to drive malate and citrate flux in response to Al stress. In addition to chelation of external Al^{3+} (Kochian et al., 2004; Ma, 2007), the protection provided by released OAs on active sites in the cell wall from Al binding is considered as another efficient strategy to increase Al resistance (Li et al., 2009). Interestingly, Al-induced callose accumulation and hematoxylin stain were weakened in the root-apex MZ of the *vha-a2 vha-a3* mutant compared with those in the wild type, whereas they were similar in the root-apex DTZ of these plants (Figs. 1C and 2B), which is the target site of Al toxicity in roots. The local distribution patterns indicate that enhanced Al resistance in *vha-a2 vha-a3* roots may be related to the protection of cell walls located at the MZ from Al^{3+} binding facilitated by secretion of malate and citrate. Second, exogenous application of malate and citrate phenocopied the effects of VHA-a2 and VHA-a3 mutation on root growth under Al stress (Fig. 7). Third, consistent with the role of VHA-a2 and VHA-a3 mutation, addition of ConcA, a vacuolar H^+ pump inhibitor, enhanced Al resistance in the wild type. However, this addition did not rescue Al-induced inhibition of primary root growth of the *almt1* mutant (Fig. 8), suggesting that ALMT1 plays a vital role in defective V-ATPase–induced Al resistance. Moreover, the *vha-a2 vha-a3* mutant displayed enhanced up-regulation of *ALMT1* and *MATE* expression under Al stress, accompanied by an increase in *STOP1* expression and a decrease in *WRKY46* expression (Fig. 8; Supplemental Fig. S11A). Such responses were reported to contribute to a more active PM-localized transport system responsible for root malate and citrate excretion (Hoekenga et al., 2006; Kobayashi et al., 2007; Liu et al., 2009). In addition, analysis of the expression patterns of *ALS3* and *STAR1* genes and the growth phenotypes of *als3* and *star1* mutants upon Al stress demonstrated that these two tonoplast-localized proteins are not required for defective V-ATPase–induced Al resistance, although they are crucial for Al resistance (Larsen et al., 2005, 2007; Huang et al., 2010; Dong et al., 2017; Wang et al., 2019). Finally, we proposed that Al resistance in the *vha-a2 vha-a3* mutant is not related to tolerance of Pi deficiency, because limitation of Pi supply did not phenocopy nor abolish the longer primary root phenotype observed in the *vha-a2 vha-a3* mutant in response to Al stress (Supplemental Fig. S12). Importantly, after exposure to Al toxicity, neither Pi content in roots and shoots nor the expression levels of representative low-Pi responsive genes of *vha-a2 vha-a3* plants were higher than those of wild-type plants (Supplemental Fig. S12). In addition, Al-induced changes in Fe accumulation in *vha-a2 vha-a3* mutant root tips, namely, higher internal Fe content and similar external Fe distribution pattern compared with that of the wild type (Supplemental Fig. S13), do not appear to agree with the notion that higher Fe levels contribute to root growth inhibition in Pi-deprived plants (Ward et al., 2008; Müller et al., 2015; Balzergue et al., 2017; Dong et al., 2017; Mora-Macías et al., 2017; Godon et al., 2019; Wang et al., 2019). Since Pi and Fe play important roles in root Al responses, such changes in Pi and Fe demand more in-depth examination to determine how these two ions regulate *vha-a2 vha-a3* mutant responses to Al stress. Taken together, these results suggest that V-ATPase is suppressed to promote OAs exudation to detoxify external Al^{3+} and not for vacuolar Al sequestration.

Although the central importance of OAs in external Al detoxification has long been recognized (Kochian et al., 2004; Ma, 2007; Meyer et al., 2010), the exact source of a burst of OAs in the root exudates after exposure to Al stress remains to be fully understood. In our study, we also collected data to determine the mechanisms underlying Al-induced elevated secretion of malate and citrate in *vha-a2 vha-a3* mutant root exudates. We found that the transcriptional abundance of malate and citrate metabolism genes was similar between the wild type and the *vha-a2 vha-a3* mutant (Supplemental Fig. S10). Moreover, *vha-a2 vha-a3* mutant roots contained no more malate and citrate content than that in wild-type roots under Al treatment, although elevated secretion of malate and citrate was observed in *vha-a2 vha-a3* mutant root exudates (Fig. 7). These results are consistent with the notion that Al-induced elevated secretion of malate and citrate in root exudates poorly associates with internal OAs metabolism (Hayes and Ma, 2003). In plants, the majority of malate and citrate is typically stored in vacuoles, where they function in osmoregulation and as counterions (Martinoia and Rentsch, 1994; Marty, 1999; Meyer et al., 2010), alongside a H^+ electrochemical gradient across the tonoplast that is predominantly maintained by V-ATPase (Sze et al., 1999; Gaxiola et al., 2007; Schumacher and Krebs, 2010). On the other hand, we found that Al-induced OAs secretion was coupled with dramatic decreases in *VHA-a2* and *VHA-a3* expression. These decreases could significantly reduce OAs storage in the vacuoles as previously reported in maize (*Zea mays*) roots (Garzón et al., 2011). In this context, *vha-a2 vha-a3* mutant roots lost the major V-ATPase activity (Fig. 3; Krebs et al., 2010; Tang et al., 2012),

suggesting that OAs transport into the vacuoles is severely impaired and that alternative pathways are required for these OAs to efflux. Indeed, we found that Al-induced up-regulation of *ALMT1* and *MATE* was further enhanced when VHA-a2 and VHA-a3 were disrupted (Fig. 8; Supplemental Figure S11). These data also demonstrate that defective V-ATPase not only inhibits OAs transport into the vacuoles but also enhances OAs flux into the apoplastic space. Interestingly, we also found that ALMT1 mutation and addition of anion transporter inhibitor 9-AC, which damage OAs transport across the PM, overrode Al-induced suppression of *VHA-a2* and *VHA-a3* expression (Fig. 9). These results thus reveal an antagonistic relationship between cytosolic OAs transport across these two membrane systems. As a result, during Al toxicity-induced root growth inhibition, Arabidopsis roots strategically suppress vacuolar H^+-ATPase activity to reduce OAs storage in the vacuoles, and this coupled with increases in PM-localized OAs transporter activity thereby redirects sufficient intracellular OAs into the apoplast.

Another important factor for cytosol-apoplast OAs transport is a well-established H^+ gradient across the PM, which is largely maintained by AHA-type H^+-ATPase (Zhang et al., 2017). Although low pH values were found to up-regulate *ALMT1* transcripts (Kobayashi et al., 2013; Godon et al., 2019) and mediate OAs secretion from the roots (Pellet et al., 1997; Degenhardt et al., 1998; Larsen et al., 1998; Shen et al., 2005), the mechanisms underlying root growth regulation by PM H^+-ATPase under Al stress remain largely unknown. Here, we defined the role of PM H^+-ATPase in Al-induced inhibition of root growth by regulating OAs flux. We found that PM H^+-ATPase activity was activated upon Al treatment and that this activation was further enhanced when V-ATPase was defective. For example, compared to the wild type, *vha-a2 vha-a3* mutant roots displayed an increase in several characteristics associated with enhanced PM H^+-ATPase activity, including higher H^+ pump activity in root PM vesicles, higher expression levels of *AHA1*, *AHA2*, and *AHA7* (Fig. 4), and more H^+ exudation in the apoplast (Supplemental Fig. S6). In addition, visualization of local H^+ distribution by fluorescent pH indicator HPTS indicated that increased H^+ exudation was largely detected in the *vha-a2 vha-a3* root-apex meristem part (Fig. 6), which is consistent with the observation that this part accumulated less Al (Fig. 2). Further genetic analysis of plants with altered PM H^+-ATPase activity showed that the increase in PM H^+-ATPase activity contributed to the enhanced Al resistance in *vha-a2 vha-a3* mutants (Figs. 4 and 5). After determining that this increase is not sufficient to confer Al resistance (Supplemental Figs. S7 and S8), we examined possible changes in OAs transport in plants with altered PM H^+-ATPase activity. We found that, upon Al treatment, changes in malate and citrate content in *vha-a2 vha-a3* root exudates positively correlated with the activity of PM H^+-ATPase. Furthermore, addition of the PM H^+-ATPase inhibitor vanadate reduced the secretion

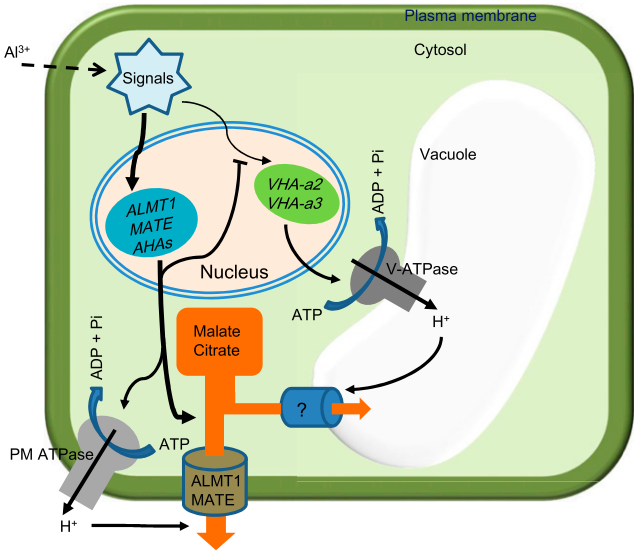

Figure 10. Schematic model of interaction of V-ATPase with AHAs, ALMT1, and MATE in driving Al-induced cytosol OAs efflux into vacuole lumen or apoplastic space. In response to Al stress, a preferred activation of *AHAs*, *ALMT1*, and *MATE* transcripts over *VHA-a2* and *VHA-a3* transcripts is triggered to drive cytosol OAs efflux into apoplastic space. As a result, considerable amounts of cytosolic OAs are distributed to the apoplastic space for detoxifying Al externally, and VHA-a2 and VHA-a3 are inhibited to reduce OAs transport into the vacuole. When the OAs distribution into apoplastic space is impaired, VHA-a2 and VHA-a3 are reversibly activated to drive cytosol OAs into vacuole lumen. The question mark (?) indicates the unknown transporters located at the tonoplast.

of malate and abolished the Al resistance of the *vha-a2 vha-a3* mutant (Figs. 5 and 7). Interestingly, the response patterns of PM H^+-ATPase to Al-induced suppression of V-ATPase activity were similar to those of ALMT1 (Figs. 3 and 8), suggesting that PM H^+-ATPase and ALMT1 function downstream of defective V-ATPase–associated signaling. We thus propose that activated PM H^+-ATPase induces an enhanced apoplastic H^+ gradient across PM that, in turn, coordinates with PM-localized transporters to efficiently deliver intracellular OAs into the apoplastic space to maintain root growth upon Al treatment.

In conclusion, the results of this study have uncovered a previously unrecognized Al exclusion mechanism facilitated by OAs allocation by vacuolar-type H^+-ATPase. As central intermediates in plant metabolism, malate and citrate are strictly synthesized and well distributed in the vacuoles. On the other hand, root internal malate and citrate have been found to be readily mobilized into soils when plants are exposed to multiple environmental stimuli (Meyer et al., 2010). Integrating our data, we proposed a model in which tonoplast- and PM-localized OAs transport systems antagonistically function in determining external Al exclusion or internal Al tolerance (Fig. 10). This model shows that, in response to Al stress, *AHAs*, *ALMT1*, and *MATE* transcripts are preferentially activated over

VHA-a2 and *VHA-a3* transcripts, thereby promoting cytosol OAs efflux into the apoplastic space to detoxify external Al^{3+}. Meanwhile, this cytosol-apoplast OAs transport suppresses *VHA-a2* and *VHA-a3* expression. When this transport is impaired, VHA-a2 and VHA-a3 are reversibly activated to drive cytosol OAs into the vacuole lumen, leading to internal Al tolerance. At present, we do not know the detailed molecular mechanisms underlying the converse regulation of these PM- and tonoplast-localized OAs transport systems. Recent work suggests that the malate shuttle serves as a communication signal from organelles, presumably via balancing of cellular ATP/NAD(P)H (Zhao et al., 2018), the substrates of H^+ pumps. It would be interesting to investigate whether the malate shuttle is involved in fine-tuning H^+ pumps for the direction of Al-regulated cytosolic OAs flux in the future.

MATERIALS AND METHODS

Plant Materials and Growth Conditions

Arabidopsis (*Arabidopsis thaliana*) wild type (ecotype Columbia-0) and the transfer DNA insertion mutants *vha-a2* (SALK_142642), *vha-a3* (SALK_029786), and *aha2-4* (CS67807) were obtained from the Arabidopsis Biological Resource Center, and the mutant *avp1-4* (GK-596F06) was obtained from the European Arabidopsis Stock Centre. The mutants *vha-a2 vha-a3* (Tang et al., 2012), *det3* (Schumacher et al., 1999), and *almt1* (Hoekenga et al., 2006) were described in previous studies. Homozygous individuals were screened by PCR using the primers listed in Supplemental Table S1. The *vha-a2 vha-a3 avp1-4* triple mutant and the *vha-a2 vha-a3 aha2* triple mutant were generated by genetic crosses of *vha-a2 vha-a3* with *avp1-4* or with *aha2-4*, respectively. Homozygous *vha-a2 vha-a3* plants in F2 populations were isolated by scoring the specific phenotype of the mutant and then screened by PCR using the primers listed in Supplemental Table S1, and the F3 and later generations were used for analyses.

For on-plate growth assays, seeds were sterilized with 75% (v/v) ethanol for 5 min, washed in sterilized water three times, and sown on half-strength Murashige and Skoog or one-sixth strength Murashige and Skoog medium containing 1% (w/v) Suc (Sigma-Aldrich) and solidified with 1% (w/v) agar (Sigma-Aldrich). The pH was buffered by 2 mM Homo-PIPES (Sigma-Aldrich) as described previously by Hoekenga et al. (2006) to 4.5, unless otherwise stated. To examine effects of Pi, the Pi concentration in the normal medium (200 μM) was increased to 2 mM or decreased to 20 μM. The plates were incubated at 4°C in darkness for 2 d and then were positioned vertically. On day 11 after germination, the seedlings were imaged to measure primary root lengths using ImageJ software (https://imagej.nih.gov/ij/) or were collected to weigh biomass. For hydroponic cultures, 4-week-old seedlings after germination on half-strength Murashige and Skoog plates were transferred to nonbuffered one-sixth strength Murashige and Skoog solutions at initial pH 4.5. The plants were grown at 22°C in growth chambers with a 16-h light/8-h dark photoperiod.

RT-PCR and RT-qPCR Analyses

Total RNA was extracted from plant roots using TRIzol reagent (Invitrogen), followed by synthesis of poly(dT) cDNA using the Moloney murine leukemia virus reverse transcriptase (Promega). RT-qPCR was performed using the SYBR Green I Master kit (Roche Diagnostics) according to the manufacturer's instructions on a CFX Connect real-time system (Bio-Rad). qPCR on each sample was repeated in triplicate. *ACTIN2* (AT3G18780) was used as the internal standard in both RT-PCR and RT-qPCR analyses. All primers used are listed in Supplemental Table S1.

Measurements of Al, Pi, and Fe Contents by ICP-MS

Four-week-old Arabidopsis seedlings were transferred onto one-sixth strength Murashige and Skoog solutions (pH 4.5 buffered with Homo-PIPES) without or with 250 μM $AlCl_3$. After 72 h of treatment, wild-type and mutant seedlings were collected and pooled into roots and shoots. After washing with distilled water three to five times, the samples were dried for 48 h at 80°C, milled to fine powder, weighed, and digested with concentrated HNO_3 (Sigma-Aldrich) in a digester (DigiBlock ED16, LabTech). Ion concentration was measured by ICP-MS (NexION 300, Perkin-Elmer). Each sample was tested at least three times.

Observations of Root-Apex Structure, Hematoxylin Staining, Perls/Diaminobenzidine Staining, and Morin Fluorescence

To observe root-apex structure, the 7-d-old seedlings sown on the one-sixth strength Murashige and Skoog agar without or with 250 μM $AlCl_3$ were immersed in a drop of the solution (4 g of chloral aldehyde in 1 mL of glycerol and 2 mL of water) and were observed under a microscope (BX53, Olympus). To observe hematoxylin staining and morin fluorescence signals, 7-d-old seedlings sown on half-strength Murashige and Skoog were incubated in one-sixth strength Murashige and Skoog solutions at pH 4.5 supplemented with 0 or 150 μM $AlCl_3$ for 6 h and were then stained using one-sixth strength Murashige and Skoog solutions without Al^{3+}, pH 4.5, containing 2 mg/mL hematoxylin, 0.2 mg/mL KIO_3, or 100 μM morin (Sigma-Aldrich) for 30 min. After rinsing with water three times, the root tips were observed under a microscope (BX53, Olympus). Perls/diaminobenzidine staining on 7-d-old plant roots was performed as described previously by Dong et al. (2017).

Measurements of Vacuolar and PM H^+ Pump Activities

Five-week-old Arabidopsis plants were transferred into one-sixth strength Murashige and Skoog solutions, pH 4.5, supplemented with 0 or 250 μM $AlCl_3$. After 3 d of treatment, roots of the plants were collected to prepare tonoplast vesicles as described previously (Tang et al., 2012), or to prepare microsomal PMs as described previously (Shen et al., 2005). The V-ATPase and V-PPase activity of 10 μg of microsomal vesicles was determined as Pi release after 40 min of incubation at 28°C. The V-ATPase and V-PPase assay solutions were used as described previously (Tang et al., 2012). Wavelengths of the UV spectrophotometer (BioMate 3S, Thermo Fisher Scientific) used for colorimetric measurement of V-ATPase and V-PPase activity were 355 and 355 nm, respectively.

To prepare PM vesicles, 20 g of roots was collected from 5-week-old Arabidopsis plants incubated in one-sixth strength Murashige and Skoog solutions containing different Al^{3+} concentrations for 3 d. Isolation of the PM was performed according to the method of Shen et al. (2005). We used 10 μM vanadate to evaluate feasibility and found the vanadate-sensitive ATPase occupied 85% of the total activity in the PM fraction. PM H^+-ATPase activity was measured at a wavelength of A_{700} as described previously (Shen et al., 2005).

Measurements of Apoplastic pH Values

To measure the pH in the solutions, 36 5-week-old seedlings were transferred into 400 mL of one-sixth strength Murashige and Skoog solutions with initial pH 5.4 supplemented with 250 μM $AlCl_3$. After treatment, solutions were collected for pH measurement by pH indicator (FE28, Mettler Toledo).

To detect apoplastic H^+ secretion, HPTS staining was used to visualize apoplastic pH as described previously (Barbez et al., 2017), with modification. Briefly, 7-d-old Arabidopsis seedlings were transferred into one-sixth strength Murashige and Skoog solutions, pH 5.0, without or with 150 μM $AlCl_3$ for 6 h and then incubated in the one-sixth strength Murashige and Skoog solutions, pH 5.0, containing 1 mM HPTS for 30 min. After rinsing with water three times, the roots of seedlings were observed under a confocal microscope (LSM-710, Leica). The protonated HPTS form (excitation, 405 nm; emission peak, 514 nm) and deprotonated HPTS form (excitation, 458 nm; emission peak, 514 nm) were detected as described in a previous study (Barbez et al., 2017). Image analysis was performed using the Fiji software (fiji.sc). The experiments described were performed in at least three biological repetitions.

Measurements of Malate and Citrate Content

Root malate and citrate exudation was detected as described previously by Ding et al. (2013). Briefly, 36 5-week-old Arabidopsis seedlings were transferred into 400 mL of one-sixth strength Murashige and Skoog solutions, pH 4.5, without or with 250 μM $AlCl_3$. After 3 d of incubation, the solutions were

collected and passed through cation- and anion-exchange columns filled with 10 g of resin-001X and 5 g of Dowex 1×8 chloride form (100–200-μm mesh, Sigma-Aldrich). After elution with 10 mL of 1 M HCl, the eluate was concentrated in a rotary evaporator at 40°C. The residue was redissolved in 1 mL of deionized ultrapure water and was used to detect malate and citrate concentration by HPLC (model 1200SL, Agilent Technologies).

To measure root internal malate and citrate content, 5-week-old plants were incubated in one-sixth strength Murashige and Skoog solutions, pH 4.5, without or with 250 μM $AlCl_3$. After 3 d of incubation, the roots were collected to prepare crude samples. Two grams of roots was ground at 4°C with 10 mL of cold water, and the homogenate was filtered through four layers of cheesecloth and centrifuged at 4,950*g* for 10 min. The supernatant was then centrifuged one more time. The supernatant was collected to be concentrated in a rotary evaporator at 70°C. The residue was redissolved in 1 mL of deionized ultrapure water for HPLC analysis.

Statistical Analysis

For all experiments, at least three independent repetitions were performed. Data were subjected to statistical analyses using one- or two-way ANOVA followed by Student's *t* test or Tukey's honestly significant difference (HSD) mean-separation test (Supplemental Table S2).

Accession Numbers

Sequence data from this article can be found in The Arabidopsis Information Resource database under the following accession numbers: AHA1 (AT2G18960); AHA2 (AT4G30190); AHA3 (AT5G57350); AHA4 (T3G47950); AHA7 (AT3G60330); AHA8 (AT3G42640); AHA10 (AT1G17260); AHA11 (AT5G62670); ACTIN2 (AT3G18780); ALMT1 (AT1G08430); ALS1 (AT5G39040); ALS3 (AT2G37330); AVP1 (AT1G15690); CSY1 (AT3G58740); CSY3 (AT2G42790); LPR1 (AT1G23010); MATE (AT1G51340); MDH1 (AT1G04410); MMDH1 (AT1G53240); MMDH2 (AT3G15020); NLA (AT1G02860); PHO1 (AT3G23430); PHT1;1 (AT5G43350); PHT1;4 (AT2G38940); PMDH1 (AT2G22780); STOP1 (AT1G34370); STAR (AT1G67940); VHA-a2 (AT2G21410); VHA-a3 (AT4G39080); WRKY45 (AT3G01970); WRKY46 (AT2G46400).

Supplemental Data

The following supplemental materials are available.

Supplemental Figure S1. Phenotypic analysis of metals sensitivity in *vha-a2 vha-a3* mutant in the medium with pH 5.8 or pH 4.3.

Supplemental Figure S2. Phenotypic analysis of *vha-a2 vha-a3* mutant under various conditions of $Al_2(SO_4)_3$.

Supplemental Figure S3. Phenotypic analysis of Al^{3+} sensitivity in *vha-a2* or *vha-a3* mutant.

Supplemental Figure S4. Effect of mutation of AVP1 on Al^{3+} sensitivity.

Supplemental Figure S5. Phenotypic analysis of Al^{3+} sensitivity in *det3* mutant.

Supplemental Figure S6. Effects of wild type and *vha-a2 vha-a3* mutant on pH values of the solutions containing 250 μM Al^{3+}.

Supplemental Figure S7. Phenotypic analysis of *vha-a2 vha-a3* mutant grown under the medium with different initial pH values.

Supplemental Figure S8. Phenotypic analysis of *vha-a2 vha-a3* mutant grown under the buffered medium to various pH values.

Supplemental Figure S9. Standard curves of malate and citrate detected by HPLC analysis.

Supplemental Figure S10. Effect of aluminum stress on the expression levels of malate and citrate metabolism genes.

Supplemental Figure S11. ALS3 and STAR1 are not required for Al resistance induced by defective V-ATPase.

Supplemental Figure S12. The response to low-Pi stress does not contribute to Al resistance in *vha-a2 vha-a3* mutant.

Supplemental Figure S13. Iron accumulation in the wild-type and *vha-a2 vha-a3* mutant roots.

Supplemental Table S1. Primers used in this study.

Supplemental Table S2. Statistical analysis tables.

ACKNOWLEDGMENTS

We thank Chaofeng Huang (Shanghai Center for Plant Stress Biology) for the *almt1*, *als3*, and *star1* mutants; Yingbai Shen (Beijing Forestry University) for the *aha2-4* mutant; and K Schumacher (University of Heidelberg) for *vha-a2 vha-a3* mutant seeds. We thank Fangjie Zhao (Nanjing Agricultural University) for advice on ICP-MS analysis and the Jiangsu Collaborative Innovation Center for Modern Crop Production for technical support.

Received May 24, 2019; revised July 18, 2019; accepted July 18, 2019; published July 31, 2019.

LITERATURE CITED

Ahn SJ, Sivaguru M, Osawa H, Chung GC, Matsumoto H (2001) Aluminum inhibits the H(+)-ATPase activity by permanently altering the plasma membrane surface potentials in squash roots. Plant Physiol **126:** 1381–1390

Balzergue C, Dartevelle T, Godon C, Laugier E, Meisrimler C, Teulon JM, Creff A, Bissler M, Brouchoud C, Hagège A, et al (2017) Low phosphate activates STOP1-ALMT1 to rapidly inhibit root cell elongation. Nat Commun **8:** 15300

Barbez E, Dünser K, Gaidora A, Lendl T, Busch W (2017) Auxin steers root cell expansion via apoplastic pH regulation in *Arabidopsis thaliana*. Proc Natl Acad Sci USA **114:** E4884–E4893

Belal R, Tang R, Li Y, Mabrouk Y, Badr E, Luan S (2015) An ABC transporter complex encoded by Aluminum Sensitive 3 and NAP3 is required for phosphate deficiency responses in Arabidopsis. Biochem Biophys Res Commun **463:** 18–23

Bose J, Babourina O, Shabala S, Rengel Z (2010) Aluminium-induced ion transport in Arabidopsis: The relationship between Al tolerance and root ion flux. J Exp Bot **61:** 3163–3175

Cho D, Villiers F, Kroniewicz L, Lee S, Seo YJ, Hirschi KD, Leonhardt N, Kwak JM (2012) Vacuolar CAX1 and CAX3 influence auxin transport in guard cells via regulation of apoplastic pH. Plant Physiol **160:** 1293–1302

Degenhardt J, Larsen PB, Howell SH, Kochian LV (1998) Aluminum resistance in the Arabidopsis mutant alr-104 is caused by an aluminum-induced increase in rhizosphere pH. Plant Physiol **117:** 19–27

Delhaize E, Ryan PR, Randall PJ (1993) Aluminum tolerance in wheat (*Triticum aestivum* L.): II. Aluminum-stimulated excretion of malic acid from root apices. Plant Physiol **103:** 695–702

Ding ZJ, Yan JY, Xu XY, Li GX, Zheng SJ (2013) WRKY46 functions as a transcriptional repressor of ALMT1, regulating aluminum-induced malate secretion in Arabidopsis. Plant J **76:** 825–835

Dong J, Piñeros MA, Li X, Yang H, Liu Y, Murphy AS, Kochian LV, Liu D (2017) An Arabidopsis ABC transporter mediates phosphate deficiency-induced remodeling of root architecture by modulating iron homeostasis in roots. Mol Plant **10:** 244–259

Eggert DA (1970) Th use of morin for fluorescent localization of aluminum in plant tissues. Stain Technol **45:** 301–303

Eticha D, Stass A, Horst WJ (2005) Localization of aluminium in the maize root apex: Can morin detect cell wall-bound aluminium? J Exp Bot **56:** 1351–1357

Ferjani A, Segami S, Horiguchi G, Muto Y, Maeshima M, Tsukaya H (2011) Keep an eye on PPi: The vacuolar-type H+-pyrophosphatase regulates postgerminative development in Arabidopsis. Plant Cell **23:** 2895–2908

Garzón T, Gunsé B, Moreno AR, Tomos AD, Barceló J, Poschenrieder C (2011) Aluminium-induced alteration of ion homeostasis in root tip vacuoles of two maize varieties differing in Al tolerance. Plant Sci **180:** 709–715

Gaxiola RA, Palmgren MG, Schumacher K (2007) Plant proton pumps. FEBS Lett **581:** 2204–2214

Godon C, Mercier C, Wang X, David P, Richaud P, Nussaume L, Liu D, Desnos T (2019) Under phosphate starvation condition, Fe and Al

trigger the transcription factor STOP1 to accumulate in the nucleus of Arabidopsis root cells. Plant J **99:** 937–949

Harper JF, Manney L, DeWitt ND, Yoo MH, Sussman MR (1990) The *Arabidopsis thaliana* plasma membrane H(+)-ATPase multigene family. Genomic sequence and expression of a third isoform. J Biol Chem **265:** 13601–13608

Hayes JE, Ma JF (2003) Al-induced efflux of organic acid anions is poorly associated with internal organic acid metabolism in triticale roots. J Exp Bot **54:** 1753–1759

Hoekenga OA, Vision TJ, Shaff JE, Monforte AJ, Lee GP, Howell SH, Kochian LV (2003) Identification and characterization of aluminum tolerance loci in Arabidopsis (Landsberg erecta x Columbia) by quantitative trait locus mapping. A physiologically simple but genetically complex trait. Plant Physiol **132:** 936–948

Hoekenga OA, Maron LG, Piñeros MA, Cançado GM, Shaff J, Kobayashi Y, Ryan PR, Dong B, Delhaize E, Sasaki T, et al (2006) AtALMT1, which encodes a malate transporter, is identified as one of several genes critical for aluminum tolerance in Arabidopsis. Proc Natl Acad Sci USA **103:** 9738–9743

Horst WJ, Püschel AK, Schmohl N (1997) Induction of callose formation is a sensitive marker for genotypic aluminium sensitivity in maize. Plant Soil **192:** 23–30

Huang CF, Yamaji N, Ma JF (2010) Knockout of a bacterial-type ATP-binding cassette transporter gene, AtSTAR1, results in increased aluminum sensitivity in Arabidopsis. Plant Physiol **153:** 1669–1677

Illés P, Schlicht M, Pavlovkin J, Lichtscheidl I, Baluska F, Ovecka M (2006) Aluminium toxicity in plants: Internalization of aluminium into cells of the transition zone in Arabidopsis root apices related to changes in plasma membrane potential, endosomal behaviour, and nitric oxide production. J Exp Bot **57:** 4201–4213

Iuchi S, Koyama H, Iuchi A, Kobayashi Y, Kitabayashi S, Kobayashi Y, Ikka T, Hirayama T, Shinozaki K, Kobayashi M (2007) Zinc finger protein STOP1 is critical for proton tolerance in Arabidopsis and coregulates a key gene in aluminum tolerance. Proc Natl Acad Sci USA **104:** 9900–9905

Kobayashi Y, Hoekenga OA, Itoh H, Nakashima M, Saito S, Shaff JE, Maron LG, Piñeros MA, Kochian LV, Koyama H (2007) Characterization of AtALMT1 expression in aluminum-inducible malate release and its role for rhizotoxic stress tolerance in Arabidopsis. Plant Physiol **145:** 843–852

Kobayashi Y, Kobayashi Y, Sugimoto M, Lakshmanan V, Iuchi S, Kobayashi M, Bais HP, Koyama H (2013) Characterization of the complex regulation of AtALMT1 expression in response to phytohormones and other inducers. Plant Physiol **162:** 732–740

Kochian LV (1995) Cellular mechanisms of aluminum toxicity and resistance in plants. Annu Rev Plant Physiol Plant Mol Biol **46:** 237–260

Kochian LV, Hoekenga OA, Pineros MA (2004) How do crop plants tolerate acid soils? Mechanisms of aluminum tolerance and phosphorous efficiency. Annu Rev Plant Biol **55:** 459–493

Krebs M, Beyhl D, Görlich E, Al-Rasheid KA, Marten I, Stierhof YD, Hedrich R, Schumacher K (2010) Arabidopsis V-ATPase activity at the tonoplast is required for efficient nutrient storage but not for sodium accumulation. Proc Natl Acad Sci USA **107:** 3251–3256

Larsen PB, Degenhardt J, Tai CY, Stenzler LM, Howell SH, Kochian LV (1998) Aluminum-resistant Arabidopsis mutants that exhibit altered patterns of aluminum accumulation and organic acid release from roots. Plant Physiol **117:** 9–18

Larsen PB, Geisler MJ, Jones CA, Williams KM, Cancel JD (2005) ALS3 encodes a phloem-localized ABC transporter-like protein that is required for aluminum tolerance in Arabidopsis. Plant J **41:** 353–363

Larsen PB, Cancel J, Rounds M, Ochoa V (2007) Arabidopsis ALS1 encodes a root tip and stele localized half type ABC transporter required for root growth in an aluminum toxic environment. Planta **225:** 1447–1458

Li J, Yang H, Peer WA, Richter G, Blakeslee J, Bandyopadhyay A, Titapiwantakun B, Undurraga S, Khodakovskaya M, Richards EL, Krizek B, Murphy AS, et al (2005) Arabidopsis H+-PPase AVP1 regulates auxin-mediated organ development. Science **310:** 121–125

Li YY, Zhang YJ, Zhou Y, Yang JL, Zheng SJ (2009) Protecting cell walls from binding aluminum by organic acids contributes to aluminum resistance. J Integr Plant Biol **51:** 574–580

Liang C, Piñeros MA, Tian J, Yao Z, Sun L, Liu J, Shaff J, Coluccio A, Kochian LV, Liao H (2013) Low pH, aluminum, and phosphorus coordinately regulate malate exudation through GmALMT1 to improve soybean adaptation to acid soils. Plant Physiol **161:** 1347–1361

Lin WY, Huang TK, Chiou TJ (2013) Nitrogen limitation adaptation, a target of microRNA827, mediates degradation of plasma membrane-localized phosphate transporters to maintain phosphate homeostasis in Arabidopsis. Plant Cell **25:** 4061–4074

Liu J, Magalhaes JV, Shaff J, Kochian LV (2009) Aluminum-activated citrate and malate transporters from the MATE and ALMT families function independently to confer Arabidopsis aluminum tolerance. Plant J **57:** 389–399

Ma JF (2007) Syndrome of aluminum toxicity and diversity of aluminum resistance in higher plants. Int Rev Cytol **264:** 225–252

Ma JF, Ryan PR, Delhaize E (2001) Aluminium tolerance in plants and the complexing role of organic acids. Trends Plant Sci **6:** 273–278

Magalhaes JV, Liu J, Guimarães CT, Lana UG, Alves VM, Wang YH, Schaffert RE, Hoekenga OA, Piñeros MA, Shaff JE, et al (2007) A gene in the multidrug and toxic compound extrusion (MATE) family confers aluminum tolerance in sorghum. Nat Genet **39:** 1156–1161

Martinoia E, Rentsch D (1994) Malate compartmentation-responses to a complex metabolism. Annu Rev Plant Physiol Plant Mol Biol **45:** 447–467

Marty F (1999) Plant vacuoles. Plant Cell **11:** 587–600

Matsumoto H (1988) Inhibition of proton transport activity of microsomal membrane vesicles of barley roots by aluminium. Soil Sci Plant Nutr **34:** 499–506

Meyer S, De Angeli A, Fernie AR, Martinoia E (2010) Intra- and extracellular excretion of carboxylates. Trends Plant Sci **15:** 40–47

Miyasaka SC, Buta JG, Howell RK, Foy CD (1991) Mechanism of aluminum tolerance in snapbeans: Root exudation of citric Acid. Plant Physiol **96:** 737–743

Mora-Macías J, Ojeda-Rivera JO, Gutiérrez-Alanís D, Yong-Villalobos L, Oropeza-Aburto A, Raya-González J, Jiménez-Domínguez G, Chávez-Calvillo G, Rellán-Álvarez R, Herrera-Estrella L (2017) Malate-dependent Fe accumulation is a critical checkpoint in the root developmental response to low phosphate. Proc Natl Acad Sci USA **114:** E3563–E3572

Müller J, Toev T, Heisters M, Teller J, Moore KL, Hause G, Dinesh DC, Bürstenbinder K, Abel S (2015) Iron-dependent callose deposition adjusts root meristem maintenance to phosphate availability. Dev Cell **33:** 216–230

Osawa H, Matsumoto H (2002) Aluminium triggers malate-independent potassium release via ion channels from the root apex in wheat. Planta **215:** 405–412

Palmgren MG (2001) Plant plasma membrane H+-ATPases: Powerhouses for nutrient uptake. Annu Rev Plant Physiol Plant Mol Biol **52:** 817–845

Pellet DM, Papernik LA, Jones DL, Darrah PR, Grunes DL, Kochian LV (1997) Involvement of multiple aluminum exclusion mechanisms in aluminum resistance in wheat. Plant Soil **192:** 63–68

Polle E, Konzak CF, Kittrick JA (1978) Visual detection of aluminium tolerance levels in wheat by hematoxylin staining of seedling roots. Crop Sci **18:** 823–827

Rasi-Caldogno F, De Michelis MI, Pugliarello MC, Marrè E (1986) H-pumping driven by the plasma membrane ATPase in membrane vesicles from radish: Stimulation by fusicoccin. Plant Physiol **82:** 121–125

Roschzttardtz H, Conéjéro G, Curie C, Mari S (2009) Identification of the endodermal vacuole as the iron storage compartment in the Arabidopsis embryo. Plant Physiol **151:** 1329–1338

Ryan PR, DiTomaso JM, Kochian LV (1993) Aluminium toxicity in roots: An investigation of spatial sensitivity and the role of the root cap. J Exp Bot **44:** 437–446

Sasaki T, Yamamoto Y, Ezaki B, Katsuhara M, Ahn SJ, Ryan PR, Delhaize E, Matsumoto H (2004) A wheat gene encoding an aluminum-activated malate transporter. Plant J **37:** 645–653

Schumacher K, Krebs M (2010) The V-ATPase: Small cargo, large effects. Curr Opin Plant Biol **13:** 724–730

Schumacher K, Vafeados D, McCarthy M, Sze H, Wilkins T, Chory J (1999) The Arabidopsis det3 mutant reveals a central role for the vacuolar H(+)-ATPase in plant growth and development. Genes Dev **13:** 3259–3270

Segami S, Tomoyama T, Sakamoto S, Gunji S, Fukuda M, Kinoshita S, Mitsuda N, Ferjani A, Maeshima M (2018) Vacuolar H^+-pyrophosphatase and cytosolic soluble pyrophosphatases cooperatively regulate pyrophosphate levels in *Arabidopsis thaliana*. Plant Cell **30:** 1040–1061

Seidel T, Siek M, Marg B, Dietz KJ (2013) Energization of vacuolar transport in plant cells and its significance under stress. Int Rev Cell Mol Biol **304:** 57–131

Shen H, He LF, Sasaki T, Yamamoto Y, Zheng SJ, Ligaba A, Yan XL, Ahn SJ, Yamaguchi M, Sasakawa H, Matsumoto H (2005) Citrate secretion coupled with the modulation of soybean root tip under aluminum stress. Up-regulation of transcription, translation, and threonine-oriented phosphorylation of plasma membrane H+-ATPase. Plant Physiol **138:** 287–296

Shen R, Ma JF, Kyo M, Iwashita T (2002) Compartmentation of aluminium in leaves of an Al-accumulator, *Fagopyrum esculentum* Moench. Planta **215:** 394–398

Shin H, Shin HS, Dewbre GR, Harrison MJ (2004) Phosphate transport in Arabidopsis: Pht1;1 and Pht1;4 play a major role in phosphate acquisition from both low- and high-phosphate environments. Plant J **39:** 629–642

Sivaguru M, Horst WJ (1998) The distal part of the transition zone is the most aluminium-sensitive apical root zone of *Zea mays* L. Plant Physiol **116:** 155–163

Stefanovic A, Ribot C, Rouached H, Wang Y, Chong J, Belbahri L, Delessert S, Poirier Y (2007) Members of the PHO1 gene family show limited functional redundancy in phosphate transfer to the shoot, and are regulated by phosphate deficiency via distinct pathways. Plant J **50:** 982–994

Svistoonoff S, Creff A, Reymond M, Sigoillot-Claude C, Ricaud L, Blanchet A, Nussaume L, Desnos T (2007) Root tip contact with low-phosphate media reprograms plant root architecture. Nat Genet **39:** 792–796

Sze H, Li X, Palmgren MG (1999) Energization of plant cell membranes by H+-pumping ATPases. Regulation and biosynthesis. Plant Cell **11:** 677–690

Tang RJ, Liu H, Yang Y, Yang L, Gao XS, Garcia VJ, Luan S, Zhang HX (2012) Tonoplast calcium sensors CBL2 and CBL3 control plant growth and ion homeostasis through regulating V-ATPase activity in Arabidopsis. Cell Res **22:** 1650–1665

Tang RJ, Zhao FG, Garcia VJ, Kleist TJ, Yang L, Zhang HX, Luan S (2015) Tonoplast CBL-CIPK calcium signaling network regulates magnesium homeostasis in Arabidopsis. Proc Natl Acad Sci USA **112:** 3134–3139

Ueno K, Kinoshita T, Inoue S, Emi T, Shimazaki K (2005) Biochemical characterization of plasma membrane H+-ATPase activation in guard cell protoplasts of *Arabidopsis thaliana* in response to blue light. Plant Cell Physiol **46:** 955–963

Vazquez MD, Poschenrieder C, Corrales I, Barcelo J (1999) Change in apoplastic aluminum during the initial growth response to aluminum by roots of a tolerant maize variety. Plant Physiol **119:** 435–444

Wang BL, Shen JB, Zhang WH, Zhang FS, Neumann G (2007) Citrate exudation from white lupin induced by phosphorus deficiency differs from that induced by aluminum. New Phytol **176:** 581–589

Wang H, Xu Q, Kong YH, Chen Y, Duan JY, Wu WH, Chen YF (2014) Arabidopsis WRKY45 transcription factor activates PHOSPHATE TRANSPORTER1;1 expression in response to phosphate starvation. Plant Physiol **164:** 2020–2029

Wang X, Wang Z, Zheng Z, Dong J, Song L, Sui L, Nussaume L, Desnos T, Liu D (2019) Genetic dissection of Fe-dependent signaling in root developmental responses to phosphate deficiency. Plant Physiol **179:** 300–316

Ward JT, Lahner B, Yakubova E, Salt DE, Raghothama KG (2008) The effect of iron on the primary root elongation of Arabidopsis during phosphate deficiency. Plant Physiol **147:** 1181–1191

Wissemeir AH, Klotz F, Horst WJ (1987) Aluminum induced callose synthesis in roots of soybean (*Glycine max* L.). J Plant Physiol **129:** 487–492

Yang Y, Tang RJ, Mu B, Ferjani A, Shi J, Zhang H, Zhao F, Lan WZ, Luan S (2018) Vacuolar proton pyrophosphatase is required for high magnesium tolerance in *Arabidopsis.* Int J Mol Sci **19:** E3617

Zhang J, Wei J, Li D, Kong X, Rengel Z, Chen L, Yang Y, Cui X, Chen Q (2017) The role of the plasma membrane H^+-ATPase in plant responses to aluminum toxicity. Front Plant Sci **8:** 1757

Zhao Y, Luo L, Xu J, Xin P, Guo H, Wu J, Bai L, Wang G, Chu J, Zuo J, et al (2018) Malate transported from chloroplast to mitochondrion triggers production of ROS and PCD in *Arabidopsis thaliana*. Cell Res **28:** 448–461

Zheng SJ, Ma JF, Matsumoto H (1998) High aluminum resistance in buckwheat. I. Al-induced specific secretion of oxalic acid from root tips. Plant Physiol **117:** 745–751

Zhu Y, Yan F, Zörb C, Schubert S (2005) A link between citrate and proton release by proteoid roots of white lupin (*Lupinus albus* L.) grown under phosphorus-deficient conditions? Plant Cell Physiol **46:** 892–901